A new, faint population of X-ray transients

Author(s):
Bauer, Franz E.; Treister, Ezequiel; Schawinski, Kevin; Schulze, Steve; Luo, Bin; Alexander, David M.; Brandt, William N.; Comastri, Andrea; Forster, Francisco; Gilli, Roberto; Kann, David Alexander; Maeda, Keiichi; Nomoto, Ken'ichi; Paolillo, Maurizio; Ranalli, Piero; Schneider, Donald P.; Shemmer, Ohad; Tanaka, Masaomi; Tolstov, Alexey; Tominaga, Nozomu; Tozzi, Paolo; Vignali, Cristian; Wang, JunXian; Xue, Yongquan; Yang, Guang

Publication date:
2017-06

Permanent link:
https://doi.org/10.3929/ethz-b-000214966

Originally published in:
Monthly Notices of the Royal Astronomical Society 467(4), https://doi.org/10.1093/mnras/stx417

Funding acknowledgement:
138979 - From the Dawn of the Universe to Today: The Co-evolution of Galaxies and Black Holes (SNF)
166159 - From the Dawn of the Universe to Today: The Co-evolution of Galaxies and Black Holes (SNF)

Monthly Notices
of the
ROYAL ASTRONOMICAL SOCIETY

MNRAS **467,** 4841–4857 (2017)
Advance Access publication 2017 February 20

doi:10.1093/mnras/stx417

A new, faint population of X-ray transients

Franz E. Bauer,[1,2,3,4★] Ezequiel Treister,[1,4,5★] Kevin Schawinski,[6★] Steve Schulze,[2,1] Bin Luo,[7,8] David M. Alexander,[9] William N. Brandt,[10,11,12] Andrea Comastri,[13] Francisco Forster,[14,2] Roberto Gilli,[13] David Alexander Kann,[15] Keiichi Maeda,[16,17] Ken'ichi Nomoto,[17†] Maurizio Paolillo,[18,19,20] Piero Ranalli,[21] Donald P. Schneider,[10,11] Ohad Shemmer,[22] Masaomi Tanaka,[23] Alexey Tolstov,[17] Nozomu Tominaga,[24] Paolo Tozzi,[25] Cristian Vignali,[26,13] Junxian Wang,[27] Yongquan Xue[27] and Guang Yang[10,11]

Affiliations are listed at the end of the paper

Accepted 2017 February 15. Received 2017 February 14; in original form 2016 November 6

ABSTRACT

We report on the detection of a remarkable new fast high-energy transient found in the Chandra Deep Field-South, robustly associated with a faint ($m_{\rm R} = 27.5$ mag, $z_{\rm ph} \sim 2.2$) host in the CANDELS survey. The X-ray event is comprised of 115^{+12}_{-11} net 0.3–7.0 keV counts, with a light curve characterized by an ≈100 s rise time, a peak 0.3–10 keV flux of $\approx 5 \times 10^{-12}$ erg s^{-1} cm^{-2} and a power-law decay time slope of -1.53 ± 0.27. The average spectral slope is $\Gamma = 1.43^{+0.23}_{-0.13}$, with no clear spectral variations. The X-ray and multiwavelength properties effectively rule out the vast majority of previously observed high-energy transients. A few theoretical possibilities remain: an 'orphan' X-ray afterglow from an off-axis short-duration gamma-ray burst (GRB) with weak optical emission, a low-luminosity GRB at high redshift with no prompt emission below ∼20 keV rest frame, or a highly beamed tidal disruption event (TDE) involving an intermediate-mass black hole and a white dwarf with little variability. However, none of the above scenarios can completely explain all observed properties. Although large uncertainties exist, the implied rate of such events is comparable to those of orphan and low-luminosity GRBs as well as rare TDEs, implying the discovery of an untapped regime for a known transient class, or a new type of variable phenomena whose nature remains to be determined.

Key words: gamma-ray burst: general – galaxies: active – X-rays: bursts – X-rays: general.

1 INTRODUCTION

The ever-improving depth and sky coverage of modern telescopes have opened the floodgates to the transient universe and enabled the discovery and characterization of several new classes of exotic variable phenomena over the past decades (e.g. Klebesadel, Strong & Olson 1973; Bade, Komossa & Dahlem 1996; Galama et al. 1998; Kouveliotou et al. 1998; Gezari et al. 2006; Lorimer et al. 2007; Soderberg et al. 2008; Bloom et al. 2011; Thornton et al. 2013; Garnavich et al. 2016). A distinct subset of such variable and transient objects can only be understood from their high-energy properties as determined by past and current space missions (e.g. *CGRO*, *Einstein*, *ROSAT*, *ASCA*, *BeppoSAX*, *HETE-2*, *RXTE*, *INTEGRAL*, *Chandra*, *XMM–Newton*, *Swift*, *NuSTAR*). While the bulk of X-ray transients relate to accretion processes on to black holes (BHs), neutron stars (NSs) and white dwarfs (WDs), there are several emerging classes of exotic X-ray transients whose nature and driving mechanisms remain unclear or unknown (e.g. Metzger et al. 2011; Woosley & Heger 2012; Loeb, Shvartzvald & Maoz 2014; Tchekhovskoy et al. 2014; Zhang 2014; Ciolfi 2016; Irwin et al. 2016). Such objects provide critical challenges to our conventional paradigms, and offer the potential for insight into poorly understood physics.

Here we report the discovery of a new fast X-ray transient (FXRT) found in the *Chandra* Deep Field-South (CDF-S). The unique multiwavelength properties of this transient appear to set it apart from any known class of variable observed to date, suggesting that the event either represents a new class of X-ray transient or probes a

★ E-mail: fbauer@astro.puc.cl (FEB); etreiste@astro.puc.cl (ET); keven.schawinksi@phys.ethz.ch (KS)
† Hamamutsu Professor

new regime for a previously known class. While the estimated rate of such transients remains modest and subject to large uncertainties, their origin could have implications for future high-energy and/or gravitational wave (GW) searches.

We have organized the paper as follows: Data and analysis methods are detailed in Section 2; possible interpretations are discussed in Section 3; rate estimates are assessed in Section 4; and finally, a summary and exploration of future prospects is given in Section 5. We adopt a Galactic neutral column density of $N_{\rm H} = 8.8 \times 10^{19}$ cm^{-2} (Kalberla et al. 2005) towards the direction of the transient. Unless stated otherwise, errors are quoted at 1σ confidence, assuming one parameter of interest. All magnitudes are reported in the AB system.

2 DATA AND ANALYSIS

We describe below the primary data sets used to detect and characterize the transient, as well as to detail the variety of constraints obtained.

2.1 *Chandra* 0.3–10 keV on 2014 October 01

The CDF-S is the deepest survey of the X-ray sky, with published observations spanning 4 Ms (≈46 d; Xue et al. 2011) and an additional 3 Ms added in 2014–2016 (Chandra proposal number: 15900132; PI: W. N. Brandt). While analysing the new CDF-S ACIS-I X-ray data in near real-time, we discovered an FXRT (Luo, Brandt & Bauer 2014) mid-way through one of the observations starting in 2014 October 01 07:04:37 UT (obsid 16454, ∼50 ks exposure). X-ray analysis was performed using CIAO (v4.6) tools and custom software. Details regarding the data processing, cleaning, photometry and alignment to the alignment to the VLA radio and TENIS near-infrared astrometric reference frame can be found in Xue et al. (2011) and Luo et al. (2017). We rule out all previously known *Chandra* instrumental effects; the transient has a normal event grade and energy distribution, and is detected in many dozens of individual pixels tracing out portions of *Chandra*'s 32 × 32 pixels (16 arcsec × 16 arcsec) Lissajous dither pattern over a long time duration (indicating the source is celestial).

No X-rays above the background rate are detected at this position in any other individual *Chandra* or *XMM–Newton* obsid or combined event lists, which total 6.7 Ms for *Chandra* (Luo et al. 2017) and 2.6 Ms for *XMM–Newton* (Comastri et al. 2011). Here we assumed the 90 per cent encircled energy region to derive the source limit, while, for *XMM–Newton*, we adopted a circular aperture of 6 arcsec radius. These limits imply quiescent 0.3–10, 0.3–2.0 and 2–10 keV flux limits of 3.1×10^{-17}, 1.6×10^{-17} and 5.4×10^{-17} erg cm^{-2} s^{-1}, respectively, at 3σ confidence. The first count from CDF-S XT1 arrives ≈16.8 ks into the observation, offering immediate precursor 0.3–10, 0.3–2.0 and 2–10 keV flux limits of 5.2×10^{-15}, 2.9×10^{-15} and 7.9×10^{-15} erg cm^{-2} s^{-1}, respectively.

The transient has a J2000 position of $\alpha = 53.^{\circ}161\,550$, $\delta = -27.^{\circ}859\,353$ and an estimated 1σ positional uncertainty of 0.26 arcsec. We extracted 115 net counts in the 0.3–7 keV band for the transient from a 3 arcsec radius circular aperture (97 per cent encircled energy fraction at 1.5 keV at the source position and zero expected background counts), from which we constructed an X-ray light curve (Fig. 1) and spectrum (Fig. 2) following standard procedures. We arbitrarily set the light-curve zero-point as 10 s prior to the arrival of the first photon.

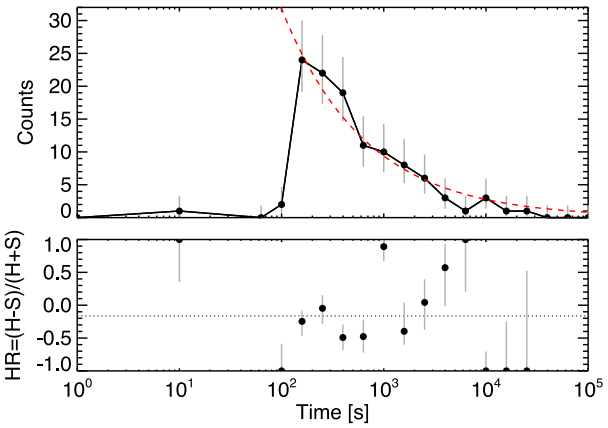

Figure 1. X-ray light curve (top panel) and hardness ratio (bottom panel) of CDF-S XT1. To highlight the sharp rise at ≈110 s, the 0.3–7.0 keV counts are logarithmically binned and shown with 1σ errors (Gehrels 1986); for this reason, binning here differs somewhat from that provided in Table 1. The red dashed curve denotes the best-fitting power-law decay time slope of $a = -1.53$. The hardness ratio, HR, and 1σ errors are calculated as $(H - S)/(H + S)$ following the Bayesian method of Park et al. (2006), where S and H correspond to the 0.3–2.0 and 2.0–7.0 keV counts, respectively. We omit bins with no counts in the bottom panel, since HR values are completely unconstrained. The dotted horizontal line signifies the HR value expected for a $\Gamma = 1.43$ power law.

The count rate of the transient near the peak of its X-ray light curve is ≈0.3–0.4 cts s^{-1} (equivalent to a readout of $\gtrsim$1 count per 3.2 s frame). As such, there is some potential for photons to suffer pile-up (two incident photons count as one higher energy photon or possibly even rejected), which would harden the spectrum and lower the observed count rate at early times. Fortunately, the transient lies at an off-axis angle of 4.3 arcmin from the ACIS-I aimpoint, and thus has an extended point spread function (PSF), such that only ≈50 per cent of the photons lie within ≈1.0–1.2 arcsec (for energies of 1.5–6.4 keV, respectively). Such a PSF should be ≈4 times less affected by pile-up compared to an on-axis PSF, implying that CDF-S XT1 should be minimally affected by pile-up (a few per cent at most). We verified this result empirically by examining the source frame by frame and based on simulations with the MARX (Davis et al. 2012).

The X-ray light curve (Fig. 1) shows a fast rise of 110 ± 50 s to a peak 0.3–10 keV flux of 5.1×10^{-12} erg s^{-1} cm^{-2} and a power-law decay of the form $F_{0.3-10\,\rm keV} = F_0(t/t_0)^a$, where t is time, $F_0 = 0.364 \pm 0.083$ erg s^{-1} cm^{-2}, $t_0 = 146 \pm 12$ s and slope $a = -1.53 \pm 0.27$, fit using a least-squares method. Dividing the light curve into logarithmic time bins of 0.2 dex, we see marginal evidence for spectral hardening in one bin around 1000 s. However, this is not strong enough to rule out a constant model at $>3\sigma$, and thus no significant spectral variations with time are found given the limited statistics (Fig. 1; see also Table 1 using Bayesian block binning). The T_{90} duration parameter, which measures the time over which the event emits from 5 per cent to 95 per cent of its total measured counts, is $5.0^{+4.2}_{-0.3}$ ks, with an associated fluence of $(4.2^{+3.5}_{-0.2}) \times 10^{-9}$ erg cm^{-2}.

Given the low number of counts, the X-ray spectrum was fit using the Cash statistic (Cash 1979) with relatively simple continuum models. The data are well fitted by either an absorbed power law ($\mathrm{d}N/\mathrm{d}E \propto E^{-\Gamma}$) with $\Gamma = 1.43^{+0.26}_{-0.15}$ or a relatively unconstrained $20.2^{+27.6}_{-11.3}$ keV absorbed thermal plasma (apec) model, with

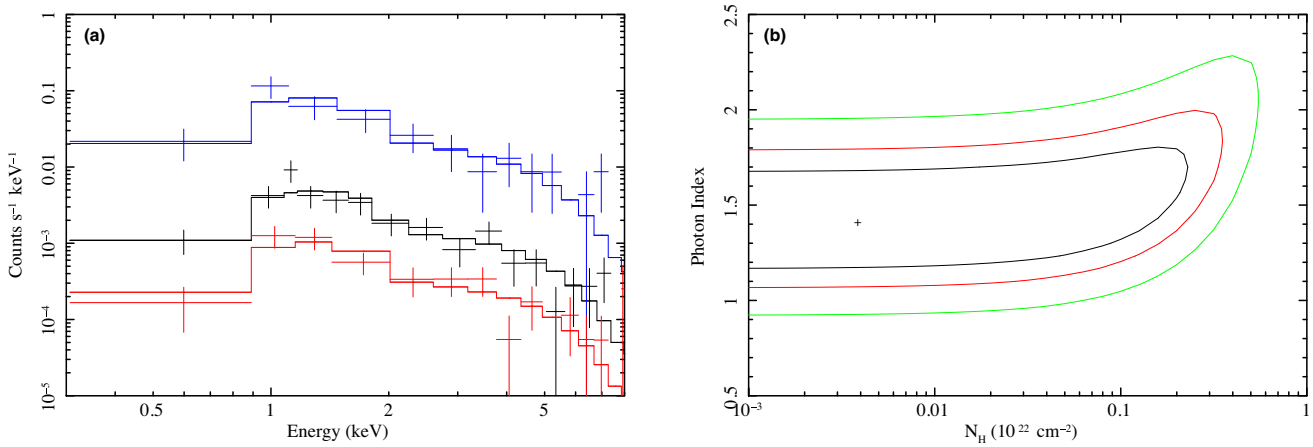

Figure 2. Best-fitting X-ray spectral model for CDF-S XT1. Panel (a): X-ray spectra (data points) and best-fitting power-law models (histogram), where the complete spectrum is denoted in black, while the early (<400 s) and late (>400 s) spectra are shown in blue and red, respectively. The best-fitting power-law model to the complete spectrum yields $\Gamma = 1.43^{+0.26}_{-0.15}$ and $N_{\rm H} < 1.5 \times 10^{21}\ (1+z)^{2.5}$ cm^{-2}. No significant evidence for spectral hardening is seen between the two epochs. Panel (b): confidence contours of Γ and $N_{\rm H}$ when modelled for the complete spectrum (1σ black, 2σ red, 3σ green).

Table 1. X-ray timing properties of CDF-S XT1. Column 1: Bayesian block time bin, in seconds, following (Scargle et al. 2013). Column 2: time bin half-width, in seconds. Column 3: 0.3–7 keV count rate, in counts s^{-1}. Column 4: 0.3–10 keV flux, in erg cm^{-2} s^{-1}. Col. 5: hardness ratio (HR) defined as $(H-S)/(H+S)$, where H and S are the 2–7 and 0.3–2 keV counts, respectively (Park et al. 2006).

Time bin	Bin half-width	CR	$F_{0.3-10\,\rm keV}$	HR
16	16	4.24×10^{-2}	$8.5^{+15.4}_{-6.4} \times 10^{-13}$	$0.23^{+0.74}_{-0.43}$
64	32	3.82×10^{-2}	$7.7^{+8.8}_{-4.6} \times 10^{-13}$	$0.50^{+0.49}_{-0.43}$
160	64	2.45×10^{-1}	$5.1^{+1.1}_{-0.9} \times 10^{-12}$	$0.21^{+0.16}_{-0.18}$
352	128	1.14×10^{-1}	$2.3^{+0.5}_{-0.4} \times 10^{-12}$	$0.14^{+0.14}_{-0.21}$
832	352	3.59×10^{-2}	$7.2^{+1.7}_{-1.4} \times 10^{-13}$	$0.07^{+0.16}_{-0.24}$
1664	480	1.03×10^{-2}	$2.1^{+0.9}_{-0.6} \times 10^{-13}$	$0.19^{+0.35}_{-0.25}$
3568	1424	3.19×10^{-3}	$6.4^{+2.9}_{-2.1} \times 10^{-14}$	$0.02^{+0.48}_{-0.33}$
18 000	13 008	2.69×10^{-4}	$5.4^{+2.9}_{-2.0} \times 10^{-15}$	$1.00^{+1.42}_{-0.00}$
138 320	12 496	3.70×10^{-5}	$7.5^{+18.7}_{-6.9} \times 10^{-16}$	$1.00^{+1.50}_{-0.00}$

a best-fitting absorption limit of $N_{\rm H} < 4.5 \times 10^{21}\ (1+z)^{2.5}$ cm^{-2} (3σ). The latter is formally consistent with the Galactic value of 8.8×10^{19} cm^{-2} (Kalberla et al. 2005), but intrinsic absorption cannot be ruled out. These values should be used with caution, as there is some possible degeneracy between the best-fitting photon index Γ and column density $N_{\rm H}$, such that a softer value of Γ ($\sim$2) cannot be excluded; see Fig. 2. The absorption limit implies $A_{\rm V} \lesssim 0.7\ (1+z)^{2.5}$ mag assuming a Galactic dust-to-gas ratio (Güver & Özel 2009), which could become substantial at large distances due to the strong redshift dependence. The observed 0.3–10 (2–10) keV flux from the total spectrum, which we extracted from the first 12 ks only to optimize the inclusion of source versus background photons, is 2.0×10^{-13} (1.4×10^{-13}) erg cm^{-2} s^{-1}.

To investigate further the possibility of spectral variance with time, we split the spectrum in two parts with roughly equal photon counts: <400 s ('early') and >400 s ('late'). This cut roughly coincides with the harder tine bin at $\sim$1000 s seen in Fig. 1. The best-fitting absorbed power-law models yielded $\Gamma_{\rm early} = 1.63^{+0.42}_{-0.21}$ and $N_{\rm H,\,early} < 7.2 \times 10^{21}(1+z)^{2.5}$ cm^{-2} at early times and $\Gamma_{\rm late} = 1.50^{+0.42}_{-0.33}$ and $N_{\rm H,\,late} < 1.0 \times 10^{22}(1+z)^{2.5}$ cm^{-2} at late times, respectively (3σ). The corresponding observed early- and late-time fluxes at 0.3–10 (2–10) keV are 2.9×10^{-12} (1.8×10^{-12}) and 4.0×10^{-14} (2.9×10^{-14}) erg cm^{-2} s^{-1}, respectively; we find a factor of $\approx$70 decrease in the 0.3–10 keV flux between the early and late regimes. If the column density $N_{\rm H}$ is left free but required to be the same at early and late times, there is no change to the early-time slope, while the late-time spectral index drops to $\Gamma_{\rm late} = 1.41^{+0.33}_{-0.23}$ with $N_{\rm H,\,early+late} < 5.5 \times 10^{21}(1+z)^{2.5}$ cm^{-2} (3σ). Again, there is no evidence for significant spectral hardening of the transient with time, within the statistical limitations of the data. Based on the confidence contours assessed for the complete spectrum, the source is consistent with Galactic absorption only, although it could be absorbed by as much as $7.2 \times 10^{21}(1+z)^{2.5}$ cm^{-2} at early times. The 2–10 keV X-ray luminosity for a variety of redshifts is provided in Table 3.

2.2 Previous imaging

The high Galactic latitude ($l = 223^\circ$, $b = -54^\circ$), low-extinction CDF-S region has been the subject of many intensive observing campaigns, and has some of the deepest coverage to date at nearly all observable wavelengths. We used in particular the images from the *Hubble Space Telescope* (*HST*) GOODS (Giavalisco et al. 2004) and CANDELS (Grogin et al. 2011; Koekemoer et al. 2011) surveys to identify and constrain the potential host galaxy of the X-ray transient. Both the CANDELS *F160W* DR1 (Guo et al. 2013) and 3D-*HST* v4.1 (Skelton et al. 2014) catalogues detect several sources in the vicinity of the X-ray transient with comparable brightnesses. We adopt values from CANDELS, which provides TFIT (Laidler et al. 2007) photometry measured on calibrated images, while 3D-*HST* fit their spectroscopic data with a set of templates and then correct the photometry; there are magnitude differences as large as $\sim$1 mag between catalogues, as well as detections in CANDELS but not in 3D-*HST*, despite clear visual confirmation. Table 2 lists the optical sources in the vicinity of the X-ray transient, in the order of distance.

Given the error in the X-ray position, source #1 is clearly the favoured counterpart and we can exclude all other detected sources

Table 2. CANDELS *F160W* Data Release 1 (DR1) catalogue parameters Column 1: object number. Column 2: CANDELS catalogue number. For completeness, the equivalent 3D-*HST* v4.1 catalogue numbers are 10718, 10709, 10670 and 10685, respectively. Column 3: J2000 right ascension and declination in degrees. Column 4: angular offset between X-ray and optical positions. Column 5: observed *R*-band magnitude. Column 6: observed *J*-band magnitude. Column 7: Kron radius. Column 8: photometry redshift and 95 per cent limit range in parentheses from best-fitting template. Column 9: absolute *R*-band magnitude. Column 10: estimated logarithm of stellar mass at best-fitting $z_{\rm ph}$. Column 11: estimated star formation rate (SFR) at best-fitting $z_{\rm ph}$.

#	CANDELS	RA, Dec.	Offset	R	J	$r_{\rm Kron}$	$z_{\rm ph}$	$M_{\rm R}$	$\log(M/{\rm M}_\odot)$	SFR (${\rm M}_\odot$ yr^{-1})
1	28573	53.161 575, −27.859 375	0.13	27.51	27.31	0.56	2.23 (0.39–3.21)	−18.7	7.99 ± 0.20	1.15 ± 0.04
2	28572	53.161 841, −27.859 427	1.09	27.38	27.34	0.50[a]	0.31 (0.07–6.81)[b]	−13.7	6.84 ± 0.18	0.40 ± 0.07
3	5438	53.161 095, −27.859 668	1.99	26.89	26.16	0.76	0.53 (0.18–2.89)	−15.5	7.82 ± 0.33	1.20 ± 0.60
4	5448	53.162 391, −27.859 707	3.29	25.78	25.27	0.69	0.15 (0.10–0.26)	−13.5	7.47 ± 0.12	0.03 ± 0.01

Notes. [a]FWHM ≈ 0.12 arcsec is consistent with point source.
[b]The photometry for 28572 can also be fit with a Galactic M-star template.

Table 3. Intrinsic constraints on CDF-S XT1 for several example redshifts. Column 1: example redshift. The photometric redshift of the nearby galaxy is nominally 2.23, but extends between 0.39 and 3.21 at 95 per cent, so we provide a wide range. Column 2: 2–10 keV X-ray luminosity within the initial 400 s, in units of 10^{45} erg s^{-1}. Column 3: absolute *F606W*-band magnitude of the tentative host galaxy. Column 4: absolute *R*-band magnitude limit for epoch E1. Column 5: absolute *R*-band magnitude limit for epoch E2. Column 6: absolute r'-band magnitude limit for epoch E3. Column 7: absolute *F110W*-band magnitude limit for epoch E4.

Redshift	$L_{2-10\,{\rm keV}}$ (10^{45} erg s^{-1})	$M_{F606W,{\rm Host}}$ (mag)	$M_{\rm R,\,E1}$ (mag)	$M_{\rm R,\,E2}$ (mag)	$M_{\rm r,\,E3}$ (mag)	$M_{F110W,{\rm E4}}$ (mag)
2.23	67.5	−18.7	>−20.5	>−19.3	>−20.3	>−17.9
0.30	0.5	−13.5	>−15.3	>−14.0	>−15.0	>−12.6
0.50	1.7	−14.8	>−16.6	>−15.3	>−16.3	>−13.9
1.00	9.4	−16.6	>−18.4	>−17.1	>−18.1	>−15.7
2.00	51.7	−18.5	>−20.3	>−19.0	>−20.0	>−17.6
3.00	138.5	−19.5	>−21.3	>−20.0	>−21.0	>−18.6

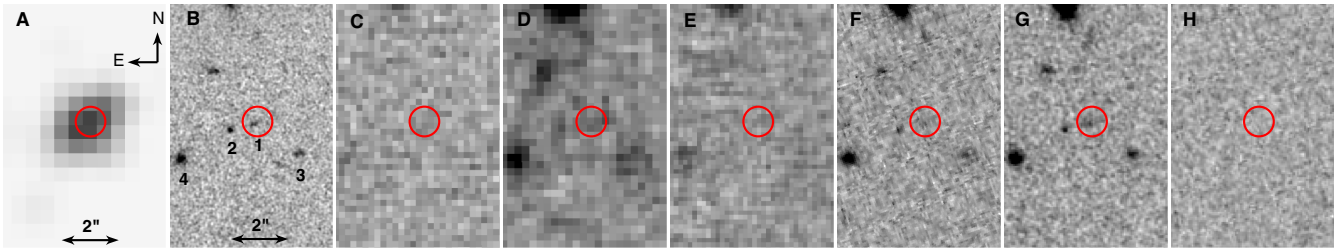

Figure 3. Images (6 arcsec × 11 arcsec) in the vicinity of CDF-S XT1. From left to right: Panel (A): *Chandra* ACIS-I 0.3–7.0 keV image of the transient detection acquired on 2014 October 01; Panel (B): *HST*/ACS *F606W* image from GOODS-S acquired prior to 2008 (Giavalisco et al. 2004); Panel (C): VLT/VIMOS *R*-band image serendipitously acquired on 2014 October 01 (80 min post-transient); Panel (D): VLT/FORS2 *R*-band image acquired on 2014 October 18 (18 d post-transient); Panel (E): Gemini/GMOS-S *r*-band image acquired on 2014 October 29 (27 d post-transient); Panel (F): *HST*/WFC3 *F110W* image acquired on 2015 January 20 (111 d post-transient); Panel (G): *HST*/WFC3 *F125W* image from CANDELS acquired prior to 2011 (Grogin et al. 2011; Koekemoer et al. 2011) and; Panel (H): *F110W* − *F125W* difference image. A 0.52 arcsec radius red circle denotes the 2σ X-ray positional error, centred on the X-ray transient position. The closest potential optical counterpart, seen clearly in the *HST* images and labelled #1 in panel (B), lies 0.13 arcsec south-east of the X-ray position and has a magnitude of $m_{\rm R} = 27.5$ mag. It is classified as a dwarf galaxy with $z_{\rm ph} = 2.23$. This galaxy appears marginally detected in the 1 h FORS2 image, but not in the VIMOS or GMOS-S images. Three other sources are labelled and discussed in the text. No transient is observed in the *HST* difference image (final panel).

at $\gtrsim$4σ. Based on the source density of the CANDELS *F160W*-band catalogue (Guo et al. 2013), the probability of a random alignment between CDF-S XT1 and a source as bright as #1 within a radius of 0.13 arcsec is <0.1 per cent.[1] At the best-fitting photometric redshift of $z_{\rm ph} = 2.23$, spectral energy distribution (SED) fitting of the CANDELS DR1 optical/near-IR (NIR) photometry suggests that the nearest counterpart is a dwarf galaxy with $M_{\rm R} = -17.3$ mag (i.e. a few times smaller than the Large Magellanic Cloud, but with a stronger star formation rate of 1.5 ${\rm M}_\odot$ yr^{-1}). The 1σ and 2σ ranges on the photometric redshift from the CANDELS *F160W*-band catalogue are 1.57–2.81 and 0.39–3.21, respectively. The reported 1σ errors on the other derived properties listed in Table 2 are only statistical, measured at the best-fitting photometric redshift, which is fixed. Incorporating the $z_{\rm ph}$ error distribution and other systematic errors, which are difficult to quantify, are likely to increase the errors substantially. The absolute magnitude of the host for a variety of redshifts is provided in Table 3. The host does not appear to be particularly dusty. Three *R*-band images and one *HST* Wide Field Camera 3 (WFC3) *F110W*-band image of the field have been acquired since the X-ray detection, spanning 0.06 and 111 d post-transient (see Fig. 3). As outlined in Sections 2.3–2.6, no clear transient counterpart is detected at $m_{\rm R} \lesssim$ 25.5–26.5 mag

[1] Even adopting a 3σ radius of 0.78 arcsec, the probability of a random match remains quite low (<4 per cent).

(Luo, Brandt & Bauer 2014; Treister, Bauer & Schawinski 2014a; Treister et al. 2014b) in the optical and $\lesssim$28.4 mag in the *F*110*W* band.

2.3 VLT/VIMOS *R* on 2014 October 1 (E1)

Serendipitously, the field of the FXRT was observed almost simultaneously (≈80 min after) at optical wavelengths by the 8.2 m Very Large Telescope (VLT) of the European Southern Observatory (ESO) using the VIsible MultiObject Spectrograph (VIMOS), as part of the VANDELS[2] public survey (PIs: R. McLure and L. Pentericci). A 550-s *R*-band image (programme ID 194.A-2003A) was obtained starting in 2014 October 1 08:20:09.6 UT with an optical seeing of ≈0.7 arcsec full width at half-maximum (FWHM) and an average airmass of 1.03 (hereafter epoch 'E1'). The data were retrieved from the ESO archive and reduced using standard procedures. After aligning the X-ray and *R*-band images to ≈0.1 arcsec, no object is detected at the location of the X-ray flare, with an estimated magnitude limit of $m_{\rm R} \approx 25.7$ mag (2σ, 0.5 arcsec radius aperture). There is evidence for a marginal detection of source #4, as seen in the deep *HST* data, but nothing fainter. No variable sources are found within at least 20–30 arcsec of the X-ray transient. The absolute magnitude limit of the transient for a variety of redshifts is provided in Table 3.

2.4 VLT/FORS2 *R* on 2014 October 19 (E2)

Following the *Chandra* detection and initial serendipitous observation, the field of the FXRT was observed again with the 8.2-m VLT using the FOcal Reducer and low dispersion Spectrograph (FORS2), 18 d after the X-ray transient was detected, as part of DDT programme 294.A-5005A (PI: Franz Bauer). A 2900-s *R*-band image was obtained starting in 2014 October 19 05:37:15.6 UT under photometric conditions with an optical seeing of ≈0.8 arcsec FWHM in the optical and an average airmass of 1.01 (hereafter epoch 'E2'). The *R* filter was chosen as a compromise between the potential expectation for a blue transient, possible obscuration, and the relative sensitivity of the detector. The ∼7 arcmin × 7 arcmin field of view (FOV) covered by FORS2 was centred on the reported coordinates of the X-ray transient. The data were retrieved from the ESO archive and reduced using standard procedures. After aligning the X-ray and *R*-band images to ≈0.1 arcsec, no source is formally detected at the position of the X-ray transient, with an estimated magnitude limit of $m_{\rm R} \approx 27.0$ mag (2σ, 0.5 arcsec radius aperture). The nearest detected source is #3. No variable sources are apparent within at least 20–30 arcsec of the X-ray transient. The absolute magnitude limit of the transient for a variety of redshifts is provided in Table 3.

2.5 Gemini-S/GMOS-S *r* on 2014 October 28 (E3)

The field of the X-ray transient was observed a third time by the 8-m Gemini-South Telescope using the imager on the Gemini Multi-Object Spectrograph (GMOS-S), 27 d after the X-ray transient was detected, as part of DDT programme GS-2014B-DD-4 (PI: Ezequiel Treister). A 4500-s *r*-band image was obtained starting at 2014 October 28 07:36:25.7 UT under clear conditions with an optical seeing of ≈0.6 arcsec FWHM and an average airmass of 1.2 (hereafter epoch 'E3'). The *r* filter was chosen as a compromise between the potential expectation for a blue transient, possible obscuration, the relative sensitivity of the detector, and to crudely match the previous two observations. With the new Hamamatsu CCDs installed, GMOS-S covers an ≈5.5 arcmin × 5.5 arcmin FOV, which was centred on the X-ray transient. The data were retrieved from the Gemini archive and reduced using standard procedures. After aligning the X-ray and *r*-band images to ≈0.1 arcsec, no source is formally detected at the position of the X-ray transient, with an estimated magnitude limit of $m_{\rm r} \approx 26.0$ mag (2σ, 0.5 arcsec radius aperture).[3] The nearest detected source to the X-ray position is #4. No variable sources are apparent within at least 20–30 arcsec of the X-ray transient. The absolute magnitude limit of the transient for a variety of redshifts is provided in Table 3.

2.6 *HST*/WFC3 *F*110*W* on 2015 January 20 (E4)

The field of the X-ray transient was observed a fourth time by *HST* using WFC3, 111 d after the X-ray transient was detected, as part of DDT programme HST-GO-14043 (PI: Franz Bauer). A 2612-s *F*110*W*-band image was obtained on 2015 January 20 11:00:13 UT, with a dithered FOV of ≈140 arcsec × 124 arcsec centred on the X-ray transient (hereafter epoch 'E4'). We switched to the *F*110*W* filter to test whether the X-ray transient might have been exceptionally red due to strong extinction or high redshift, and owing to the excellent sensitivity of this band for faint NIR emission. The data were retrieved from the Mikulski Archive for Space Telescopes and reduced using standard procedures. After aligning the X-ray and *F*110*W*-band images to ≈0.1 arcsec, we recover nearly all of the objects from the deep *HST F*125*W* image of CANDELS, including the associated counterpart source #1, with $m_{F110W} = 27.43$ mag. Based on difference imaging with the CANDELS *F*105*W* and *F*125*W* images using the High Order Transform of PSF and Template Subtraction code (Becker 2015), we place a limit of $m_{\rm F110W} \approx 28.4$ mag (2σ, 0.2 arcsec radius aperture), comparable to the expected magnitude limit based on the *HST* exposure time calculator. To place this value in context for Fig. 5, we assume a colour dependence of $m_{\rm R} - m_{F110W} \approx$0.4–0.7 mag based on gamma-ray burst (GRB) afterglow power-law spectral slopes in the range of −0.6 to −1.1 (Kann et al. 2010, 2011) and 0.4–1.0 mag for CCSNe between $z = 0.0$ and 1.0 (Poznanski et al. 2002; Drout et al. 2011; Bianco et al. 2014). This implies an equivalent limit of $m_{\rm R} = 28.8$–29.4 mag. Again, no variable sources are detected within at least 20–30 arcsec of the X-ray transient. The absolute magnitude limit of the transient from the difference imaging is provided in Table 3 for a variety of redshifts.

2.7 ATCA/CABB 2–19 GHz on 2014 October 08

Radio observations of the field of the X-ray transient were made on 2014 October 08 with the Australian Telescope Compact Array (ATCA) in the 1.5-km configuration using the Compact Array Broadband Backend at 2.1, 5, 9, 17 and 19 GHz (Burlon et al. 2014). No radio emission was detected in the vicinity of the transient, with 3σ limits of $S_{2.1\,\rm GHz} < 174$ μJy, $S_{5\,\rm GHz} < 81$ μJy, $S_{9\,\rm GHz} < 75$ μJy, $S_{17\,\rm GHz} < 105$ μJy and $S_{19\,\rm GHz} < 99$ μJy, respectively. Radio limits based on observations obtained prior to the transient are $S_{1.4\,\rm GHz} \lesssim 24$ μJy and $S_{5\,\rm GHz} \lesssim 27$ μJy (Miller et al. 2013; Burlon et al. 2014).

[2] http://vandels.inaf.it

[3] This limit is roughly 0.6 mag brighter than estimated by the Gemini-South GMOS-S ITC, possibly due to early background problems associated with the newly installed Hamamatsu CCDs.

3 POSSIBLE INTERPRETATIONS

We detail below a set of possible scenarios that might produce an FXRT such as the one we observed. In many cases, we are able to exclude these scenarios based on our available multiwavelength constraints. This list may not account for every possibility and should not be interpreted as complete.

3.1 Gamma-ray bursts

One possibility is that CDF-S XT1 is connected with a GRB afterglow or a brighter GRB flare on top of an otherwise standard GRB afterglow. GRB emission is characterized by time-scales of ∼20 s for long-duration bursts and ∼0.2 s for short-duration bursts (hereafter lGRBs and sGRBs, respectively; Meegan et al. 1996). Although many questions remain, the commonly accepted lGRB model is that of a relativistically expanding fireball with associated internal and external shocks (Mészáros & Rees 1997). After generating the γ-ray emission, the expanding fireball shocks the surrounding material, producing a broad-band X-ray-to-radio afterglow that decays in time as t^{-a} with $a \sim 1.2 \pm 0.3$ unless the Doppler boosting angle of the decelerating fireball exceeds the opening angle of the associated jet, at which point the light curve is expected to steepen (a so-called jet break; Rhoads 1999; Zhang & Mészáros 2004). Alternatively, the currently favoured sGRB progenitor scenario features a compact NS–NS or an NS-BH binary merger (e.g. Eichler et al. 1989; Narayan, Paczynski & Piran 1992), induced by angular momentum and energy losses due to GW radiation resulting in a GW burst (e.g. Abbott et al. 2016). The NS–NS case could produce either a millisecond magnetar (e.g. Zhang 2013) or a BH surrounded by a hyperaccreting debris disc, while the NS-BH case should yield a larger BH with or without a debris disc, depending on whether the NS was tidally disrupted outside of the BH event horizon. When a debris disc is present, the combination of the high accretion rate and rapid rotation can lead to energy extraction via either neutrino-antineutrino annihilation or magnetohydrodynamic processes (e.g. Blandford & Znajek 1977; Rosswog & Ramirez-Ruiz 2002; Lee & Ramirez-Ruiz 2007), which, in turn, can drive a collimated relativistic outflow. The accretion event should also produce more isotropic thermal, supernova-like emission on time-scales of $\sim 10^4$–10^6 s known as a 'kilonova' (e.g. Metzger 2016; Sun, Zhang & Gao 2017). Unfortunately, with only a few dozen well-characterized sGRBs to date, the parameter range of possible properties remains rather open.

To extend the high-energy data available on the transient, we searched for a possible γ-ray counterpart in the *Swift* and *Fermi* archives. Unfortunately, neither satellite had coverage in the direction of the *Chandra* transient in the few hours surrounding CDF-S XT1 (Palmer, Krimm, Göğüş, Y. Kaneko, A. J. van der Horst, private communications), and thus it is not well constrained above 10 keV. The field was covered by the interplanetary network (Atteia et al. 1987), although no counterpart was detected with a fluence above 10^{-6} erg cm^{-2} and a peak flux limit of above 1 photon cm^{-2} s^{-1}, both in the 25–150 keV range (Hurley, private communication), which excludes any association with a strong GRB but fails to exclude a faint GRB or orphan afterglow (Yamazaki, Ioka & Nakamura 2002; Ghirlanda et al. 2015).

For comparison, we retrieved the X-ray light curves of ∼760 *Swift* GRBs with detected X-ray afterglows from the *Swift* Burst Analyser (Evans et al. 2010b). Identical to Schulze et al. (2014), we resampled these light curves on a grid defined by the observed range of X-ray brightnesses and the time-span probed by the data. If no data were available at a particular time, we interpolated between adjacent data points (but do not extrapolate). Fig. 4 presents the light curve of CDF-S XT1 compared to this *Swift* GRB distribution in grey scale.

The peak X-ray flux and full X-ray light curve of CDF-S XT1 are fainter than almost any known GRB X-ray afterglow (Dereli et al. 2015). Thus, CDF-S XT1 would need to be an intrinsically low-luminosity, misaligned or high-redshift GRB. The light-curve decay time slope of CDF-S XT1 ($a = -1.53 \pm 0.27$) appears fairly constant and marginally steeper than the median afterglow decay time slope for GRBs ($a \approx -1.2$; Evans et al. 2009; Racusin et al. 2009), while its X-ray spectral slope ($\Gamma = 1.43^{+0.26}_{-0.15}$) lies in the hardest ≈10 per cent of the standard afterglow distribution over comparable energy bands ($\Gamma \approx 1.70 \pm 0.15$; Wang et al. 2015). While few GRBs have been well characterized below 10 keV as they initially exploded, a substantial subset of lGRBs have been observed within 10–100 s of the prompt burst, at which point the low-energy tail of the prompt emission has been seen (Tagliaferri et al. 2005; Barthelmy et al. 2005); this feature is likely responsible for the steeper initial decline seen in the grey-scale histogram distributions of *Swift*-detected GRBs shown in Fig. 4.[4] Early observational constraints of sGRBs are far more difficult to obtain due to their limited durations, although they are also expected to show early contributions from the prompt emission (Villasenor et al. 2005). Thus, a critical discriminator in CDF-S XT1's X-ray light curve is its $\approx 100(1+z)^{-1}$ s rest-frame rise time (where z is redshift), which contrasts sharply with the strong early emission and spectral softening expected from both lGRBs and sGRBs. Any burst of photons associated with the prompt emission would have been detected easily by *Chandra*, if they extended below 10–20 keV in the rest frame.

During the first several hours after a GRB, the X-ray afterglow is frequently characterized by flaring episodes (Chincarini et al. 2007, 2010; Margutti et al. 2011). The peak time of CDF-S XT1 is consistent with that for GRB flares, although the spectral slope and decay time slope are on the hard and slow ends of their respective distributions. The duration of CDF-S XT1, however, is substantially longer than those seen in GRB flares (i.e. ∼10-300 s), and thus is unlikely to fit cleanly into such a scenario.

In the optical, we compare to composite *R*-band light curves derived from a data base of optical and NIR measurements of 166 GRBs with known redshifts (Kann, Klose & Zeh 2006; Kann et al. 2010, 2011; Nicuesa Guelbenzu et al. 2012). These data were gridded in an identical manner to the X-ray data; Fig. 5 shows the corresponding density distribution (cropped at a lower limit of 10^{-3} d, since that is the regime most relevant for our observed constraints and allows better visualization of the 'busy' 10–100 d region). Comparing the initial *R*-band limit ($m_R \gtrsim 25.7$ mag at ≈80 minutes post-transient) to this optical density distribution, the transient is again fainter than ≳99 per cent of known GRB afterglows. As seen in Fig. 5, the early 2σ limit lies only ∼1 mag above a $\nu^{-0.43}$ power-law extrapolation of the X-ray light curve into the optical band (dashed red curve in Fig. 5), thereby providing a relatively stringent constraint on any excess emission above this estimate. Given the prompt X-ray emission, the early limit rules out a standard off-axis jet scenario, wherein we would expect to find

[4] We note that a handful of *Swift*-detected GRBs do show initial rises and peaks around 100–500 s, similar to CDF-S XT1, but their subsequent behaviour appears quite distinct from that of CDF-S XT1, with multiple strong flares and clear breaks.

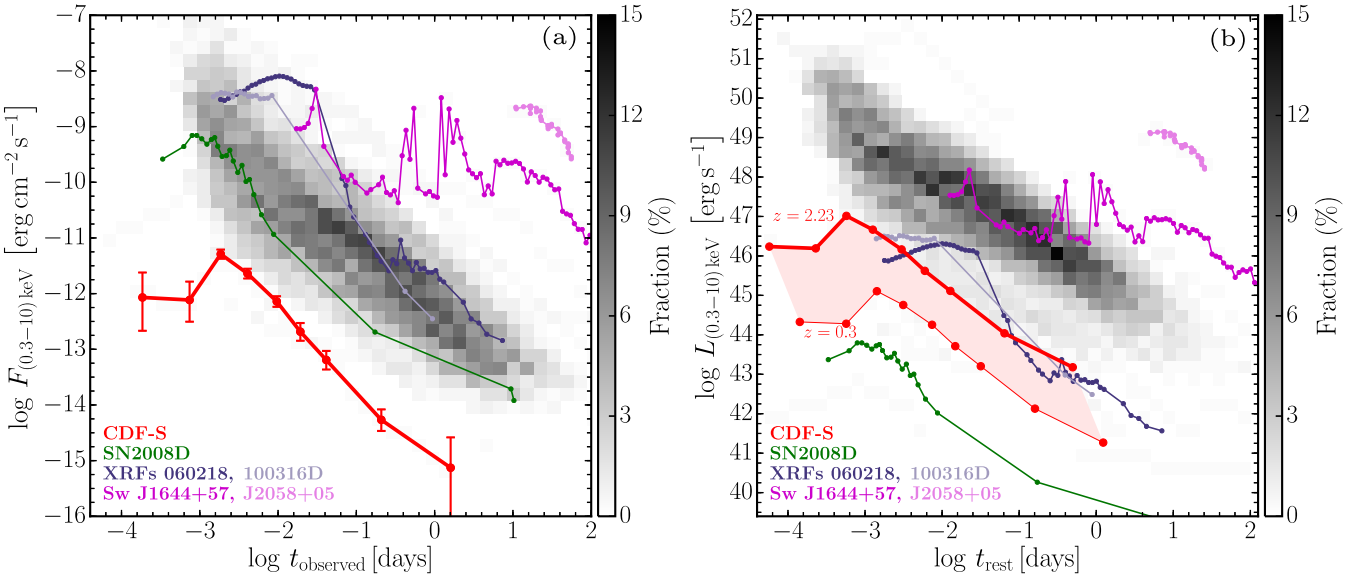

Figure 4. 0.3–10 keV light curve of CDF-S XT1, shown in panel (a) flux and panel (b) rest-frame luminosity as red points and curves (assuming a range of possible redshifts on the luminosity side). Shown in grey are the fractional 2D histogram distributions of X-ray light curves for ≈760 *Swift*/BAT detected GRBs with detected X-ray afterglows. The power-law decay time slope of CDF-S XT1 ($a = -1.53 \pm 0.27$) is marginally steeper than that of the typical GRB afterglow ($a \approx -1.2$; Evans et al. 2009; Racusin et al. 2009), while its luminosity lies at the lower bound of the GRB afterglow distribution. The $\approx 100(1+z)^{-1}$ s rise time of CDF-S XT1, however, is uncharacteristic of GRBs. A few exceptional individual XRF/SNe and beamed TDEs are also shown. Low-luminosity XRFs 080109/SN 2008D (27 Mpc), 060218/SN 2006aj (145 Mpc) and 100316D/SN 2010bh (263 Mpc) all are proposed to have SBO-driven origins (Campana et al. 2006; Soderberg et al. 2008; Modjaz et al. 2009; Starling et al. 2011; Barniol Duran et al. 2015) and lie in a similar luminosity range as CDF-S XT1, although the latter two show distinct plateaus in their early light curves that are not observed in CDF-S XT1. Relativistically beamed TDEs *Swift* J1644+57 ($z = 0.353$) and *Swift* J2058+0516 ($z = 1.185$) show similar decay time slopes over portions of their light curves, but peak much later and exhibit significant variability (Bloom et al. 2011; Cenko et al. 2012).

a relatively normal, bright optical GRB afterglow associated with weak X-ray emission (van Eerten, Zhang & MacFadyen 2010; van Eerten & MacFadyen 2011). In fact, based on synchrotron closure relations between the X-ray and optical emission, a large fraction of parameter space can be excluded. Thus, to explain the observations in a GRB scenario, the transient would need to be intrinsically low-luminosity, reddened by at least a few magnitudes, and/or at redshift $z \gtrsim 3.6$–5.0 (and hence not associated with the apparent host).

Each of these possibilities shares a relatively low probability (Jakobsson et al. 2012; Covino et al. 2013). The strong association with the $z_{\rm ph} \sim 2.2$ host galaxy appears to rule out the high redshift option and lowers the probability of the low-luminosity option. Alternatively, a small fraction of sGRBs shows extremely weak optical emission, as seen in Fig. 5, allowing an off-axis sGRB with weak optical emission to remain a viable option (Lazzati et al. 2016).

To put the radio limits into context with radio GRB afterglows, we compared the reported limits listed previously to the work of Chandra et al. (2012). In particular, the ATCA 9 GHz limit implies a faint afterglow, although a significant number of GRBs have evaded detection with deeper observations.

Based on the above considerations, the X-ray transient does not appear to be fully consistent with the properties of most known GRBs, nor the predictions for off-axis or weaker ones. The relatively low X-ray fluxes exclude all but low-luminosity, off-axis, or $z \gtrsim 4$ GRB solutions, while the optical transient limits further exclude most standard off-axis GRB solutions and necessitate weak or absorbed optical emission. The strong association with a $z_{\rm ph} \sim 2.2$ host galaxy appears to exclude the high-z solution. The lack of prompt emission below ∼20 keV rest frame further excludes any on-axis/strongly beamed scenario. Taken together, only a few tentative options may remain.

One is an 'orphan' off-axis sGRB, which, furthermore, must have exceptionally weak optical and radio emission. Based on predictions, such objects could exist, although none has yet been confirmed. Models of compact object mergers (e.g. Metzger & Piro 2014; Sun et al. 2017) suggest that the initial X-ray light curves are likely to be optically thick and 'turn-on' over time-scales of many hours to days as it expands, with peak X-ray luminosities in the range of $\sim 10^{44}$–10^{46} erg s^{-1} followed by a $\sim t^{-2}$ decay. While such peak luminosities are naively compatible with CDF-S XT1, the peak times are 2–3 dex longer. Among the many X-ray models of Sun et al. (2017), some allow for earlier turn-ons, but with correspondingly higher peak X-ray luminosities. Some compact object merger models (e.g. Metzger & Piro 2014) are additionally expected to produce strong optical/NIR emission, which we do not see. Considerable fine-tuning and/or revision of sGRB models may be required in order to more satisfactorily match the observational constraints of CDF-S XT1.

Another possibility is an explanation as a low-luminosity GRB at $z \gtrsim 2$, although the X-ray light curve and spectral properties of CDF-S XT1 remain distinct from the best-studied low-luminosity GRBs.

3.2 Shock breakout

One intriguing possibility is that the X-ray transient represents the shock breakout (SBO) from a core-collapse supernova (CCSN). An initial flash of thermal UV (or soft X-ray) radiation is expected when the CCSN shock wave emerges from the stellar surface of the

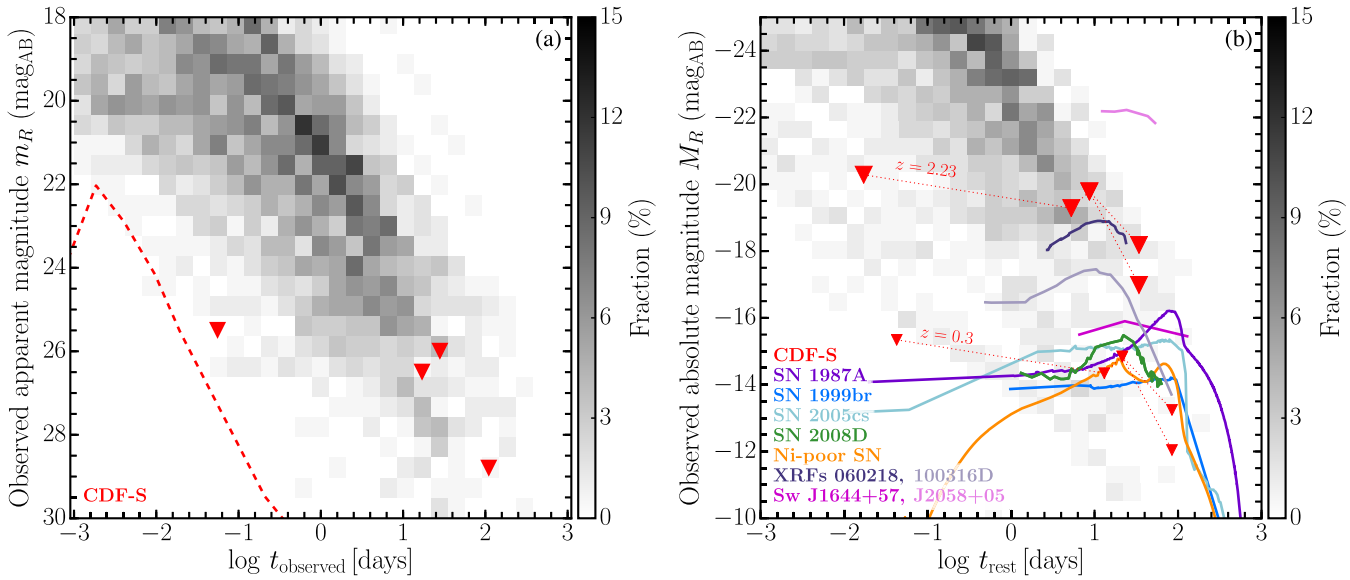

Figure 5. *R*-band (2σ) upper limits for CDF-S XT1, shown in panel (a) apparent and panel (b) absolute magnitude as solid red triangles connected with red dotted lines (assuming a range of possible redshifts on the absolute magnitude side). The *HST* *F*110*W* constraint at 111 d is displayed for the range $m_R - m_{F110W} \approx 0.4$–$1.0$ mag typical of GRBs and SNe. Shown in grey are the fractional 2D histogram distributions of *R*-band afterglow light curves for 166 GRBs with known redshifts, all corrected for Galactic extinction. The limits lie at the low end of the GRB afterglow optical distribution, with the first limit providing the strongest constraint. The dashed red curve in panel (a) shows an extrapolation of the observed X-ray light curve in Fig. 4 assuming a $\nu^{-0.43}$ power-law spectrum between the X-ray and optical regimes; the earliest limit is consistent with this, but effectively excludes any strong emission above such an extrapolation. A few exceptional individual GRBs, SN, and beamed TDEs are also shown in panel (b). Low-luminosity events like XRF 080109/SN 2008D (27 Mpc), XRF 060218/SN 2006aj (145 Mpc) and XRF 100316D/SN 2010bh (263 Mpc) can be excluded out to redshifts of ≈0.5, ≈2 and ≈1, respectively, while relativistically beamed TDEs like *Swift* J1644+57 ($z = 0.353$) and *Swift* J2058+0516 ($z = 1.185$) are excluded out to high redshift. Below $z \approx 0.5$–1.0, the *HST* limit excludes even traditionally sub-luminous or late-peaking SNe such as Type II-pec SN 1987A (50 kpc), which rises by ∼2 mag to peak quite late, Type IIP-pec SN 1999br (7.1 Mpc) and Type II-P SN 2005cs (8.6 Mpc). These three SNe are among the faintest CCSNe known (Richardson et al. 2014). In some cases, their faintness may be related to being Ni-poor CCSNe with strong fallback, for which a theoretical light curve is also shown (adopting $M_{ZAMS} = 25\,M_\odot$, $M_{Ni} = 0.02\,M_\odot$).

progenitor (Falk & Arnett 1977; Klein & Chevalier 1978; Matzner & McKee 1999; Schawinski et al. 2008; Ganot et al. 2016). The character of the SBO depends primarily on the density structure of the progenitor and the explosion energy driving the shock (Chevalier & Irwin 2011; Gezari et al. 2015), resulting in SBOs with expected initial temperatures of $\sim 10^5$ to 5×10^6 K and durations of ∼100–5000 s. The typical bolometric luminosity associated with an SBO is generally of the order of $\sim 10^{44}$–10^{45} erg s^{-1} (Ensman & Burrows 1992; Tominaga et al. 2011), while the emission in a given X-ray band (e.g. 0.3–10 or 2–10 keV) will be less (∼1–87 per cent for quoted temperature range). Moreover, a sufficiently compact progenitor with an energetic explosion could produce relativistic effects that substantially harden the X-ray spectrum and lead to significant >1 keV emission, although only for a relatively short time (1–100 s) and with dramatic spectral and temporal evolution (Tolstov, Blinnikov & Nadyozhin 2013). After the SBO, the outer layers of the star should enter an adiabatic expansion and cooling phase for ∼1–2 d, followed by a plateau phase thereafter as radiative diffusion takes over (Chevalier 1992; Popov 1993). If the stellar wind or circumstellar material (CSM) is sufficiently dense, it could intensify or prolong the SBO (by up to factors of ∼10) and delay the subsequent phases (Balberg & Loeb 2011; Moriya et al. 2011; Svirski, Nakar & Sari 2012).

While the duration of the X-ray transient is consistent with that of longer SBOs, the hard observed spectrum (e.g. $kT > 5$ keV at 3σ) appears inconsistent with the relatively low expected temperatures ($kT \sim 0.01$–1 keV) for such typical SBOs. For a fixed total energy budget from an SNe, there should be a trade-off between luminosity and temperature, whereby a larger radius at which the SBO occurs could give a higher luminosity, but a lower blackbody temperature. This makes an SBO interpretation hard to satisfy with the observed properties. The most promising models are explosions of blue supergiants like SN 1987A, which can achieve bolometric luminosities as high as 10^{45} erg s^{-1} and SEDs peaking at ∼10 keV, however, only for durations of ∼100 s (Tolstov, private communication). Alternatively, a relativistic scenario might be able to explain the observed X-ray photon index, but we do not observe the characteristic strong spectral and temporal evolution (a power-law decay time slope of $a > 2$). Additionally, by $z \sim 0.4$ the peak X-ray luminosity of the transient already exceeds the predicted bolometric peak luminosity for an SBO associated with an $E_{explosion} \approx 10^{51}$ erg progenitor. Thus, the SBO scenario is only viable at low redshift, which remains possible but unlikely based on the photometric redshift probability distribution. To accommodate the best-fitting redshift of $z = 2.23$ with an SBO scenario requires an explosion energy of $\gtrsim 10^{52}$ erg and/or an optically thick CSM.

The best-studied SBO candidate to date is X-ray flash (XRF) 080109/SN 2008D (27 Mpc), which, when compared to CDF-S XT1, has a mildly different X-ray light-curve evolution (more gradual rise, broader 'peak' and broken decline) but much softer X-ray spectrum (with $kT \sim 0.7$ keV or $\Gamma \sim 2.1$; Soderberg et al. 2008; Modjaz et al. 2009). We can also compare to the XRFs 031203/SN 2003lw (475 Mpc), 060218/SN 2006aj (145 Mpc) and 100316D/SN 2010bh (263 Mpc), which are also proposed to have SBO-driven origins. While the high-energy (>2 keV) X-ray spectral slopes over comparable bands are consistent, the latter two XRFs

show significant soft thermal components ($kT \sim 0.1$–0.2 keV), which become dominant beyond ∼1000 s (Campana et al. 2006; Starling et al. 2011; Barniol Duran et al. 2015), while CDF-S XT1 appears to marginally harden at late times.[5] In addition, the early X-ray light curves of these two events lie in stark contrast to CDF-S XT1, as they are substantially flatter and longer lasting, with steeper late time declines (Campana et al. 2006; Starling et al. 2011; Barniol Duran et al. 2015).

Another critical aspect of the SBO scenario is, of course, the expectation of subsequent strong UV/optical emission associated with the standard CCSN light curve. Our combined optical/NIR constraints, shown in Fig. 5, appear to rule out several of the faintest known SNe light curves (Richardson et al. 2014) if placed closer than $z \sim 0.5$, and more luminous ones out to $z \lesssim 1$–2, with the most critical constraints arising from the initial VIMOS and latest *HST* data points. Adopting the X-ray to optical flux ratios of XRFs 080109/SN 2008D, 031203/SN 2003lw, 060218/SN 2006aj and 100316D/SN 2010bh, the associated SNe light curves would also all have been easily detected. The most sub-luminous SNe are thought to have extremely low nickel yields (i.e. nickel masses of ≈0.002–0.075 $M_\odot$; Hamuy 2003), suggesting that if this event were an SBO, it would potentially require little nickel production, and consequently strong fallback. We also show the theoretical light curve for an Ni-poor core-collapse SN with strong fallback, from a zero-age main sequence (ZAMS) $M = 25$ $M_\odot$ progenitor and a nickel mass of 0.02 $M_\odot$. To evade the optical/NIR limits would require a rather contrived scenario of nearly complete fallback. Alternatively, if we redden the comparison light curves by $A_R = 0.3$–1.3 mag, they can fit the early ground-based limits, although all are still strongly excluded by the NIR *HST* limit at high significance unless significantly stronger reddening is assumed.

3.3 Tidal disruption event

A further possibility is that the transient was a TDE. TDEs occur when a star passes exceptionally close to a $\gtrsim 10^4$ $M_\odot$ BH (Rees 1988; Phinney 1989; Burrows et al. 2011), such that it experiences tidal forces that exceed its self-gravity, allowing the star to be shredded. Luminous thermal emission at soft X-ray through optical wavelengths is generated either by the accretion of this gas on to the BH [often limited to $L_{\rm Bol} \approx L_{\rm Edd} \approx 1.3 \times 10^{44}$ erg s^{-1} $(M_{\rm BH}/10^6\ M_\odot)$] and/or the initial shocks due to colliding stellar debris streams (Guillochon & Ramirez-Ruiz 2015). The tidal disruption radius is given by $r_{\rm TDE} \approx (2M_{\rm BH}/m_*)^{1/3} R_*$, where $M_{\rm BH}$ is the mass of the BH, while m_* and R_* are the mass and radius of the star, respectively. This radius effectively dictates in what band the thermal radiation will peak, with the effective temperature given by $T_{\rm eff} \approx 2.5 \times 10^5$ K $(M_{\rm BH}/10^6\ M_\odot)^{1/12}$ $(R_*/R_\odot)^{-1/2}$ $(m_*/M_\odot)^{-1/6}$. For normal main-sequence stars disrupted around 10^6–10^8 $M_\odot$ BHs, the radiation should peak between $T_{\rm eff} \sim 10^4$ and 10^6 K. The time-scale for the emission to rise to maximum is given by $t_{\rm min} \approx 0.11$ yr $(M_{\rm BH}/10^6\ M_\odot)^{1/2}$ $(R_*/R_\odot)^{-3/2}$ $(m_*/M_\odot)^{-1}$, after which the bolometric light curve is predicted to follow an $\approx t^{-5/3}$ power-law decay. In rare cases, material accreting on to the BH may produce a relativistic jet that gives rise to non-thermal γ-ray, X-ray and radio emission that can appear orders of magnitude more luminous and can be strongly variable (e.g. Bloom et al. 2011; Burrows et al. 2011; Cenko et al. 2012).

The decay time slope of the transient is fully consistent with the predictions for TDEs. However, the fast rise time and hard X-ray flux of CDF-S XT1 strongly exclude all 'normal' stars and supermassive BHs ($>10^6$ $M_\odot$). The only viable remaining parameter space is for a TDE comprised of a white dwarf (WD: 0.008–0.02 $R_\odot$, 1 $M_\odot$) and an intermediate-mass BH (IMBH; $\sim 10^3$–10^4 $M_\odot$), although even in such a scenario, it may be difficult to explain the hard observed X-ray spectral slope. Furthermore, the resulting Eddington luminosity for this TDE scenario would be at least two orders of magnitude too low compared to what is expected for the redshift range of the associated host galaxy (Table 3). One alternative could be that the emission arises from a relativistic jet produced by the TDE, although then we might expect substantially stronger variability fluctuations than that observed from the relatively smooth power-law decay of the transient's X-ray light curve (Levan et al. 2011). Moreover, the ratio of X-ray emission to the optical and radio limits is $\gtrsim 100$ times larger than those from the beamed TDEs *Swift* J1644+57 and *Swift* J2058+0516 (Bloom et al. 2011; Cenko et al. 2012). Moreover, the beaming requirements become quite extreme with increasing redshift. Thus, relativistically beamed emission from a TDE comprised of a WD and an IMBH remains only a remote possibility.

3.4 Galactic origin

There are at least some similarities between the reported characteristics of CDF-S XT1 and a wide variety of X-ray-emitting Galactic phenomena. We limit the discussion here only to the possibilities that have similar X-ray transient time-scales and are unlikely to require bright optical or NIR counterparts, as these are easily excluded by our imaging and line of sight through the Galaxy (for instance, this removes most high- and low-mass X-ray binary systems).

One remaining possibility is an origin as an M dwarf or brown dwarf flare. Magnetically active dwarfs (∼30 per cent of M dwarfs, ∼5 per cent of brown dwarfs) are known to flare on time-scales from minutes to hours, exhibiting flux increases by factors of a few to hundreds in the radio, optical blue, UV and/or soft X-ray (Schmitt & Liefke 2004; Mitra-Kraev et al. 2005; Berger 2006; Welsh et al. 2007). The flares can be short 'compact' ($L \lesssim 10^{30}$ erg s^{-1}, <1 h) or 'long' ($L \lesssim 10^{32}$ erg s^{-1}, ≥1 h). Flares are often recurrent on time-scales of hours to years, and in the X-ray band at least typically have thermal X-ray spectral signatures with $kT = 0.5$–1 keV, both of which are inconsistent with CDF-S XT1.[6] M dwarfs tend to be more X-ray active than brown dwarfs (Berger 2006; Williams, Cook & Berger 2014), with $\log(L_R/L_X) \sim -15.5$ in units of $\log({\rm Hz}^{-1})$ for a wide range of stars down to spectral types of about M7, after which this ratio rapidly climbs to ∼−12 for brown dwarfs. Thus, relative to the observed X-ray peak flux, the radio survey limits mentioned previously should have been more than sufficient to detect radio flares from a brown dwarf and most M dwarfs, if any occurred during the radio observations. While the best counterpart for the transient, source #1, is

[5] XRF 031203/SN 2003lw was observed in the pre-*Swift* era and hence has substantially sparser and later X-ray and optical follow-up constraints. Notably, the portions of the X-ray and optical light curves that are well sampled appear similar to those of XRF 060218/SN 2006aj (Watson et al. 2004; Mazzali et al. 2006). As such, we do not include it in Figs 4 and 5 for clarity.

[6] Although note that in some extreme RS CVn type systems, luminosities as high as $\sim 10^{34}$ erg s^{-1} and temperatures of up to ∼25 keV have been observed (e.g. Osten et al. 2016).

clearly extended in multiple images, there remains a low probability (<0.3 per cent) that that the transient could be matched to source #2, which is potentially consistent with a $m_R = 27.38$ mag M-dwarf star. Alternatively, an even fainter dwarf could lie below the *HST* detection threshold, although the low random probability of spatial coincidence with a background galaxy strongly argues against this. Notably, M dwarfs typically have absolute magnitudes of $M_R \sim 8$–14 mag (Bochanski, Hawley & West 2011), such that source #2 would have to lie at $\gtrsim$5–75 kpc (i.e. in the halo), while an undetected M dwarf would lie even further away. Similarly, brown dwarfs have typical absolute magnitudes of $M_J \sim 15$–25 (Tinney et al. 2014), such that an undetected source must lie at $\gtrsim$30 pc–3 kpc. However, such distances would imply an M-dwarf X-ray luminosity of $L_X \gtrsim (3.4\text{–}850) \times 10^{35}$ erg s^{-1} or a brown dwarf X-ray luminosity of $L_X \gtrsim (5.5\text{–}549\ 03) \times 10^{29}$ erg s^{-1}, which are at least factors of $\gtrsim 10^3$–10^5 larger than typical flares seen from M dwarfs (Pandey & Singh 2008; Pye et al. 2015) and brown dwarfs (Berger 2006), respectively. Thus, the observed transient properties appear inconsistent with those of dwarf flares.

Another possibility is that the transient was the result of a magnetar outburst. Magnetars are spinning-down, isolated NSs that have relatively slow rotation rates (∼1–10 s) and possess extremely strong magnetic fields that are considered to power characteristic and recurrent bursts of X-rays and γ-ray radiation (hence their designations as 'soft gamma repeaters', or 'anomalous X-ray pulsars' Mereghetti, Pons & Melatos 2015). They lack obvious companions from which to accrete, yet have apparent X-ray luminosities during outbursts, which can often be super-Eddington and reach luminosities as high as $\sim 10^{47}$ erg s^{-1} (Palmer et al. 2005); these cannot be explained by rotation power alone. Their strong magnetic fields are predicted to decay on time-scales of $\lesssim$10 000 yr, after which their activity ceases. Among the ≈26 magnetars known (Olausen & Kaspi 2014), many are found near OB associations and/or SN remnants and all lie in the thin disc of the Galaxy or the Magellanic clouds, implying that magnetars are possibly a rare by-product of massive O stars. Roughly half of the magnetars are persistent X-ray sources with fluxes of $\sim 10^{-14}$–10^{-10} erg s^{-1} cm^{-2} (or equivalently quiescent X-ray luminosities of the order of $\sim 10^{35}$ erg s^{-1}). The rest were primarily discovered during bright, short outbursts (0.1–1.0 s) or giant flares (0.5–40 s), ∼10–1000 times brighter than their anticipated quiescent phases, whose properties still remain relatively poorly known. The rises and decays of these outburst/flare episodes show different durations and shapes (∼1 week to months), but the decays are generally characterized by a spectral softening. The outburst duty cycle remains poorly known, as multiple distinct outburst episodes have only been detected from a few magnetars to date. The X-ray spectra are generally fit with two-component blackbody ($kT_{BB} \sim 0.5$ keV) and power-law ($\Gamma \sim 1$–4) models. A subset of magnetars have optical and radio counterparts. Based primarily on the strong association with recent star-forming regions and SN remnants (the high Galactic latitude CDF-S field is far from any known Galactic star-forming region), as well as the more sporadic and longer duration rise and decay times expected, CDF-S XT1 appears highly unlikely to be a Galactic magnetar.

Finally, the X-ray properties of CDF-S XT1 could be related to compact object such as an asteroid hitting an isolated foreground NS (Colgate & Petschek 1981; van Buren 1981; Campana et al. 2011). This possibility, which was originally suggested to explain GRBs, is difficult to rule out based on the observational data alone due to the wide parameter range of transients that can be produced. However, the combined probability that such an event occurs on an NS, which just happens to align with a faint extragalactic source to better than 1σ, is quite low (≪0.1 per cent), given an expected NS number density out to 30 kpc of ∼1000 deg^{-2} (Sartore et al. 2010) and the source density of $m_{F160W} < 27.5$ mag galaxies in the CANDELS field (0.088 arcsec^{-2}).

4 EVENT RATES

Regardless of origin, the fact that this event occurred in a pencil-beam survey field like the CDF-S naively implies a relatively high occurrence rate. However, although a handful of high-amplitude, FXRTs have been reported in the literature to date (Jonker et al. 2013; Glennie et al. 2015; De Luca et al. 2016), none appears to have the X-ray and optical transient properties of CDF-S XT1 nor an association with such a faint optical host. To quantify this, we first perform a search of the *Chandra* archive to determine the frequency of events such as CDF-S XT1, and then estimate their occurrence rate.

4.1 Comparable events

To determine the uniqueness of this transient, we conducted an archival search for similar variable events. Due to the limited variability information available (e.g. no easy access to individual source photon tables) in the most recent *XMM–Newton* 3XMM DR5 and *Swift* 1SXPS source catalogues (Evans et al. 2014; Rosen et al. 2016), we found it infeasible to assess properly whether such a source was detected by either observatory, and thus only conducted a search for similar events observed by *Chandra* using the Chandra Source Catalogue (CSC v1.17; Evans et al. 2010a). Most critically, the CSC is the only source catalogue that provides easy and straightforward access to photon event lists and light curves, which we considered absolutely essential to characterize the nature of the variability of each source. Even so, the current version of the CSC only contains relatively bright sources from the first 11 cycles (up to 2010 August 10), which factors into our rate calculations below.

We began by searching the CSC for all securely variable sources with a peak flux of $F_{2-10\,\mathrm{keV}} > 1 \times 10^{-12}$ erg s^{-1} cm^{-2} (or their count rate equivalent, adopting the best-fitting spectral slope of the transient) and which varied in flux by at least a factor of 10. This should find any similar transients down to a factor of 5 weaker than CDF-S XT1, if they exist. Such a transient should be easily detectable in virtually any *Chandra* observation. At this flux, it would also be detectable in *XMM–Newton* or *Swift*/XRT, although it might be difficult to characterize it in *Swift*/XRT data due to the typically short (1–2 ks) observations this instrument executes. The above criteria are obviously conservative, as *Chandra*'s sensitivity could allow a search up to a factor of 10 deeper. However, with so few observed counts (∼10 photons), it would be impossible to determine with much certainty whether the transient truly is similar to CDF-S XT1.

To select sources similar to CDF-S XT1, we adopted the following CSC parameters for sources observed with the ACIS-I and ACIS-S detectors, as well as the High Resolution Camera (HRC): variability probability $var\_prob > 0.9$; maximum variability count rate $o.var\_max > 0.06$ counts s^{-1}; and minimum variability count rate $o.var\_min < 0.006$ counts s^{-1}. We found 184 unique matches. Of these, 39 lie within $|b| < 10^\circ$ and are presumably Galactic in nature, while at a minimum, a further 19 and 82 can be spatially associated with Milky Way globular clusters and young star-forming regions outside the Galactic plane ($|b| > 10^\circ$), respectively. Based

on the *Chandra* positional errors, 149 candidates have Digitized Sky Survey, Two Micron All-Sky Survey and/or *Wide-Field Infrared Survey Explorer* (*WISE*) counterparts, while a further 3, 10, 8 and 4 candidates are likely associated with the Galactic plane, nearby globular clusters, star-forming regions or local galaxies, respectively, even though they do not have clear, single counterparts. In total, only nine candidates show no sign of a counterpart to the limits of these surveys, no association with extended objects and/or a location outside of the Galactic plane (hereafter *criterion #1*).

The benefit of using the CSC is that we can inspect individual data products for each catalogue source. To determine if the variability of the CSC sources shows the same basic signatures as CDF-S XT1 (i.e. non-recurrent, $\lesssim$1 ks rise, $\sim t^{-1.5}$ decline), we visually inspected and classified the X-ray light curves of all 184 sources into one of seven categories. Category 1 sources appear to be recurrent or persistent transients, exhibiting single or multiple flares, eclipses and/or gradual variations on top of otherwise quiescent rates. Recurrence/persistence was determined directly from the *Chandra* data in some cases, or based on previously known variability in the SIMBAD[7] data base catalogue. We consider category 1 sources to have distinctly different variability behaviour from CDF-S XT1 (Wenger et al. 2000).

Category 2–7 sources, on the other hand, were not considered to be recurrent or persistent transients, with only marginal or no prior and post-detection of photons during the observations. We regard this as a minimum requirement for similarity to CDF-S XT1, although we caution that such a designation is strongly dependent on how frequently a source is observed as well as the level to which an assessment of variability is carried out. Cross-matching category 2–7 sources with all known X-ray archives and carefully investigating variability across all possible instruments goes well beyond the scope of this project, and would likely result in recategorization of at least some fraction of these sources as category 1 sources.

Beyond a basic estimate of recurrence or persistence, we further divided the remaining category 2–7 sources up based on their variability properties. Category 2 sources exhibit $\gtrsim$4 ks rises and/or decay time-scales several times longer than CDF-S XT1. Category 3 sources exhibit $\sim$2–4 ks rise times and decay time-scales several times longer than CDF-S XT1 and/or flattening either early or late in the transient decay. Category 4 sources exhibit similar $\sim$2–4 ks rise times like category 3, but have time series that terminate or are of insufficient statistical quality to assess their decay rates properly. Given the strongly disparate rise and decay time-scales, category 2, 3 and 4 sources all seem unlikely to be related to CDF-S XT1.

Category 5 sources show X-ray light-curve shapes consistent with that of CDF-S XT1 with peaks of $\lesssim 10^3$ s. As such, they represent the most likely potential CDF-S XT1 analogues. Category 6 sources are similar to category 5, but have significant low-level activity in the $\sim 10^3$–$10^{4.5}$ s prior to their 'category 5' light-curve shapes. This precursor emission is not seen in CDF-S XT1 and may suggest that these objects have a different physical origin and/or are recurrent or persistent. All likely have Galactic origins. Therefore, they seem much less likely to be potential CDF-S XT1 analogues. Finally, category 7 sources exhibit weak short rise and fall behaviour within $\sim$100–500 s, and are dominated by noise at late times. Thus, they could represent fainter versions of CDF-S XT1. While two likely have Galactic origins, one is associated with a faint SDSS+*WISE* galaxy with $z_{\rm ph} \sim 0.14$ and another appears to be a strong radio source with a *WISE*-only counterpart. Neither of the latter two identification seems like a clear CDF-S XT1 analogue. In summary, after assessing the X-ray light curves of all 184 CSC candidates (hereafter *criterion #2*), we find that category 5 and 7 objects may be potential analogues, while all others categories show substantially different variability behaviour.

Finally, approximately 20–40 per cent of the 184 candidates have hardness ratios or best-fitting spectral slopes consistent with $\Gamma < 2.0$ (hereafter *criterion #3*); this fraction also holds for the candidates associated with categories 5 and 7.

A compilation of the results, broken down by category, is listed in Table 4, while the individual light curves of all category 3–7 sources are shown in Fig. 6. Factoring all three (imaging, timing and spectral) criteria together, we find that there is not a single candidate that is comparable to CDF-S XT1. For instance, among all 26 candidates in category 3–7, 21 sources appear to have a Galactic origin. Even amongst the most likely candidates in categories 5–7 that show similar light curves, roughly half have spectral slopes that are too soft, and all have an obvious Galactic or bright nearby galaxies origin. We thus conclude that transients like CDF-S XT1 appear to be rare or alternatively hard to find based on relatively simple selection criteria.

We note that Glennie et al. (2015) recently reported the detection of two unusual high-amplitude, FXRT in the *Chandra* archive, FXRT 110103 and FXRT 120830. However, both of these exhibit strong X-ray flare behaviour above constant quiescent X-ray emission of $\sim 10^{-13}$–10^{-12} erg s^{-1} cm^{-2}, which is inconsistent with the X-ray behaviour (strong quiescent limits) from CDF-S XT1. FXRT 120830 appears to be associated with a bright flare from a nearby late M or early L dwarf star, and thus appears to have a Galactic origin. FXRT 110103 lies at high Galactic latitude ($b = 32.^\circ7$) and has no counterpart to $J > 18.1$, $H > 17.6$ and $K_s > 16.3$. These limits are not too constraining and FXRT 110103 is tentatively associated by Glennie et al. with the galaxy cluster ACO 3581 at 94.9 Mpc. Jonker et al. (2013) also report the discovery of FXRT 000519, which has similar X-ray light curve properties to FXRT 110103 (including apparent quiescent emission at a flux level of $\sim 10^{-13}$–10^{-12} erg s^{-1} cm^{-2}) and is associated with M86 at 16.2 Mpc. Jonker et al. favour a tidal disruption of a WD by an IMBH, but cannot rule out alternative scenarios such as the accretion of an asteroid by a foreground NS or an off-axis GRB. Given their associations with relatively nearby galaxies, FXRT 110103 and FXRT 000519 are factors of 10^3–10^5 less luminous than CDF-S XT1, and it is not immediately obvious how they might be manifestations of the same phenomenon as CDF-S XT1. Hence, for the moment, we do not consider them to be similar.

4.2 Rate estimation

Under the above criteria, we find no transients similar to CDF-S XT1 in the entire CSC. If we relax some of the criteria, for instance, to allow for bright galaxy counterparts and a broader range of light-curve peaks, there are a few additional potential candidates that could boost the rate by up to a factor of 3–4. However, until there is a stronger understanding of the physics involved, we prefer to remain conservative. With only one detected source, the rate of such events is subject to large uncertainties. We adopt the above characterization of the CSC as our baseline and estimate the coverage of the CSC as follows.

For *Chandra*, there are two main configurations, ACIS-I and ACIS-S, with as many as six 8.5 arcmin × 8.5 arcmin detectors operational for each; in recent years, *Chandra* has advocated that users turn off at least two detectors. Alternatively, the HRC has

[7] http://simbad.u-strasbg.fr/simbad/sim-fid

Table 4. Light-curve characterization for 184 candidates from CSC search. Column 1: light-curve category (*criterion #2*). Column 2: number found. Column 3: variability characteristics. Column 4: number within $|b| \leq 10^{\circ}$ (i.e. considered Galactic). Column 5: number with clear optical counterparts or associations with globular clusters, star-forming regions, or galaxies (*criterion #1*). Column 6: number that exhibits a best-fitting X-ray spectral slope of $\Gamma < 2.0$. In many cases, the spectra and hardness ratios are not of sufficient quality to robustly determine a spectral slope. Therefore, we provide the possible range (*criterion #3*).

Cat.	#	Var. type	GalPlane?	Opt?	Hard?
1	129	Recurrent/persistent transients (flaring, eclipsing, gradual, etc.).	20	123	14–47
2	29	Non-recurrent transients with marginal or no prior/post detections; exhibit $\gtrsim$4 ks rises and/or decay time-scales several times longer than CDF-S XT1.	7	29	12
3	7	Non-recurrent transients with no prior/post detections; exhibit 2–4 ks rise times, decay time-scales several times longer than CDF-S XT1 and/or flattening either early or late in the transient decay.	3	7	4
4	5	Non-recurrent transients with no prior/post detections similar to Cat 3, but time series terminates or is of insufficient statistical quality to assess further.	2	4	2–4
5	4	Non-recurrent transients with no prior/post detections and show consistent X-ray light-curve shapes with peak of $\lesssim 10^3$.	2	4	2
6	6	Non-recurrent transients potentially similar to Cat 5, but have significant low-level activity in the $\sim 10^3$–$10^{4.5}$ s prior to Cat 5 light-curve shapes.	4	5	1–3
7	4	Non-recurrent transients with no prior/post detections; exhibit weak short rise and fall behaviour within 100–500 s and dominated by noise at late times.	1	3	0–4

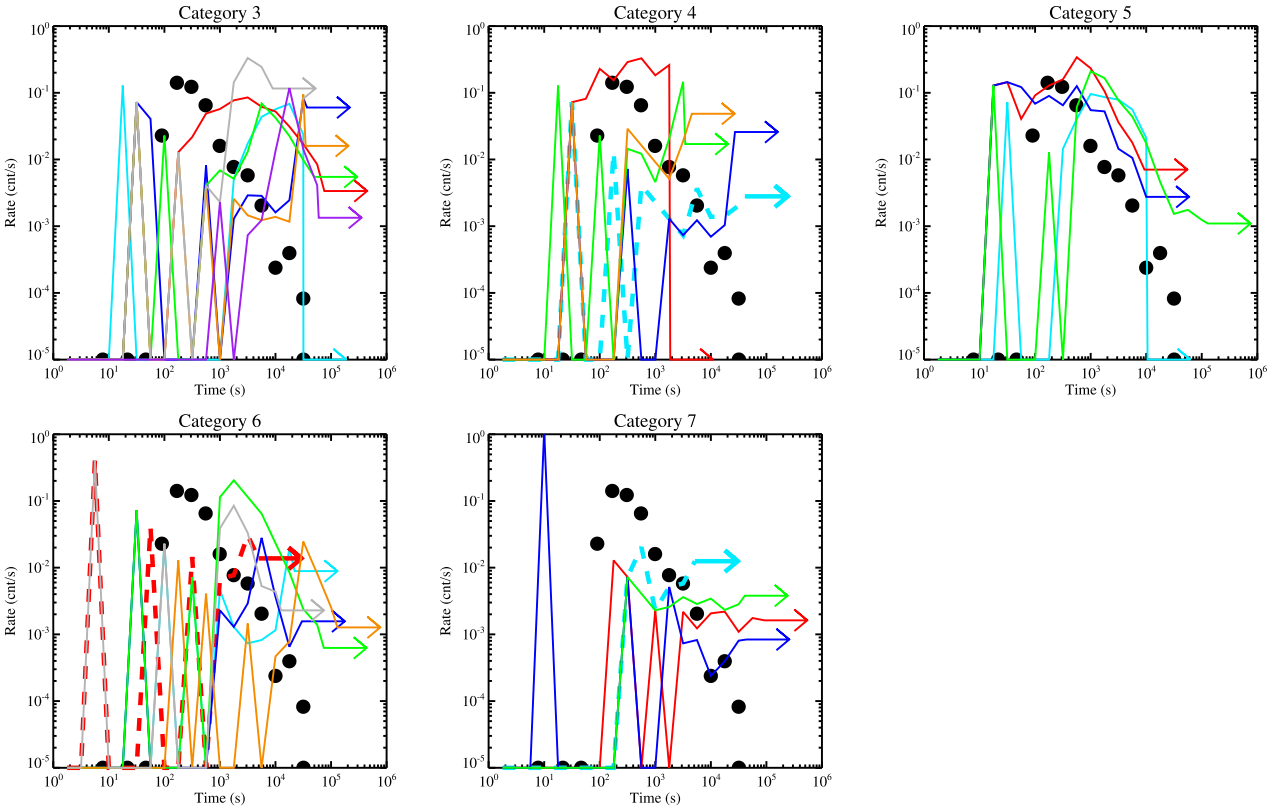

Figure 6. X-ray light curves for the 26 CSC sources classified in categories 3–7, with each panel representing a given category. The CSC light curves are all binned on the same logarithmic scale and shown without error bars for clarity. The 23 sources with and three sources without bright optical counterparts are denoted by thin solid and thick dashed lines, respectively. Based on counterpart identification, 21 sources likely have a Galactic origin. The X-ray light curve of CDF-S XT1 is shown by black circles in each panel, for comparison.

an FOV of ≈30 arcmin × 30 arcmin. The PSF and effective area of all these detectors degrade substantially beyond a few arcminutes from the aimpoint. For reference, on-axis and with the current sensitivity, a source with $F_{0.3-10\,\mathrm{keV}} = 4.2 \times 10^{-13}$ erg s^{-1} cm^{-2} and the spectral slope of the transient will yield ≈100 counts for ACIS-I, ≈150 counts for ACIS-S, and ≈64 counts for HRC in 5.0 ks, respectively. Given the degradation in sensitivity over the lifetime of *Chandra*, early cycles would have detected ≈1.5 times more photons. At 15 arcmin off-axis, vignetting alone will decrease the photon yields by ≈40 per cent for a source with $\Gamma = 1.5$, while the 90 per cent encircled energy PSF area will likewise grow by a factor of ≈400, such that considerably more background is

included. The combination of these effects makes reliable detection of a transient like CDF-S XT1 difficult beyond the primary four detectors I0-I3 for ACIS-I (289 arcmin^2), the S2+S3+S4 detectors for ACIS-S (217 arcmin^2) or the central 100 arcmin^2 for HRC. We will assume the shortest *Chandra* exposure, ≈2 ks, is sufficient to detect such a transient (and thus all *Chandra* exposures are useful), although over such short intervals it may be difficult to characterize the light curve properly.

Summing up the total on-sky exposure time (livetime) examined in the above CSC query up to 2010 August 10 with $|b| > 10^\circ$, there are 46.6, 62.1 and 3.7 Ms for the ACIS-I, ACIS-S or HRC detectors, respectively.

Such exposures imply a total potential occurrence rate of up to $4.2^{+9.7}_{-3.4}$ events deg^{-2} yr^{-1}, adopting errors following Gehrels (1986). We convert this to a volumetric rate (yr^{-1} Gpc^{-3}) in Fig. 7, assuming an increasing volume as a function of redshift between the 95 per cent confidence bounds of the photometric redshift of the associated host. Following Sun, Zhang & Li (2015), we quote event rates at the minimum peak luminosity to which they are probed. The *Chandra* observations within our CSC archive search should allow detection of 'CDF-S XT1'-like events to a peak flux limit of ∼(5–10) × 10^{-13} erg s^{-1} cm^{-2}, or a peak X-ray luminosity of ∼10^{44}–10^{46} erg s^{-1} over a redshift range of $z_{\rm ph} = 0.39$–3.21.

Although we have already largely excluded an identification with most known types of transients, it is still informative to compare the above rate to the expected rates of other major transients, such as sGRBs and lGRBs, SNe and TDEs.

For lGRBs, we adopt a simple broken power-law shape to model the intrinsic rate of beamed lGRBs (Wanderman & Piran 2010; Lien et al. 2014), assuming that they roughly trace the shape of the cosmic star formation rate as shown in Fig. 7. At $z = 0$, the rate is anchored at a value of ∼0.84 yr^{-1} Gpc^{-3} above a peak X-ray luminosity of ∼10^{49} erg s^{-1} based on simulations matched to the observed rate of lGRBs from *Swift*/BAT (Lien et al. 2014), with an uncertainty within a factor of ∼2. Given that lGRBs are thought to be beamed and highly anisotropic (Harrison et al. 1999; Levinson et al. 2002), it may be more appropriate to compare with the rate of unbeamed, or 'orphan', lGRB explosions, which should be larger by the inverse of the beaming factor. For simplicity, we adopt a beaming correction of ≈75 ± 25, based on large samples of lGRBs (Piran 2004; Guetta et al. 2005), although we caution that these corrections are often non-trivial, with low- and high-luminosity GRBs likely to have different average half-opening angles. For several well-studied lGRBs, for instance, the beaming corrections were estimated to lie between 450 and 500 (Frail et al. 2001; van Putten & Regimbau 2003), implying a much higher orphan rate and at least a factor of ∼6 to 7 uncertainty.

Given some of the potential similarities between CDF-S XT1 and the low-luminosity XRFs 060218/SN 2006aj (145 Mpc), 080109/SN 2008D (27 Mpc), and 100316D/SN 2010bh (263 Mpc), we estimate their cumulative observed rate assuming a volume of 300 Mpc, a 10 yr *Swift/BAT* search window with 90 per cent efficiency, a 2 steradian *Swift*/BAT FOV and a 10 per cent detection rate based on complex trigger criteria (Lien et al. 2014). This yields a rate of $\sim 185^{+181}_{-100}$ yr^{-1} Gpc^{-3} above a peak X-ray luminosity of ≈10^{46} erg s^{-1}, with the quoted errors being purely statistical, and likely severely underestimating systematic uncertainties. Such rates and luminosity limits are roughly consistent with the lGRB beaming factors mentioned above.

For sGRBs, there are fewer robust identifications and characterizations, leaving rate estimates substantially more uncertain. Based on available samples of ∼20 objects, the estimated observed rate is $4.1^{+2.1}_{-1.9}$ yr^{-1} Gpc^{-3} above a peak X-ray luminosity of ∼10^{49} erg s^{-1} (Wanderman & Piran 2015). The beaming corrections lie in the range of ∼70 ± 40 (Berger 2014), implying an intrinsic unbeamed or orphan sGRB rate of $\sim 290^{+530}_{-230}$ yr^{-1} Gpc^{-3} between $z = 0.1$ and 1.3 above a peak X-ray luminosity of ∼10^{47} erg s^{-1}.

For CCSNe, the rate at $z = 0$ is estimated to be ∼10^5 yr^{-1} Gpc^{-3} above a peak X-ray luminosity of ∼10^{44} erg s^{-1} and is expected to track the cosmic star formation rate as shown in Fig. 7 (Dahlen et al. 2004; Lien & Fields 2009; Taylor et al. 2014). The uncertainties are likely within a factor of ∼2 (Horiuchi et al. 2011). Based on the expected X-ray luminosities for SBOs, the local ($z < 0.5$) rates provide the most sensible comparison.

Finally, for TDEs, we note that the rates are still highly uncertain due to limited number of detections and large uncertainties in the underlying assumptions, such that estimates range of ∼300–6800 yr^{-1} Gpc^{-3} (Stone & Metzger 2016) above a peak X-ray luminosity of ∼10^{42} erg s^{-1}. The rates of TDEs accompanied by relativistic jets should be significantly smaller and with much higher X-ray luminosity limits (Bower et al. 2013; van Velzen et al. 2016).

From Fig. 7, one can see that the estimated rates for transients like CDF-S XT1 appear similar to some other transient populations. A major caveat here is that the luminosity limits for these various transient populations are quite different. After matching luminosity limits following Sun et al. (2015) and references therein, we find that the CDF-S XT1 rate is most similar to the rates of unbeamed/orphan and/or low-luminosity lGRBs and sGRBs between $z \sim 0.4$ and 2.0. This provides further indirect evidence that CDF-S XT1 may be somehow related to the GRB phenomenon. Although the rates of 'CDF-S XT1'-like events remain highly uncertain, we note that they are still likely to be substantially more common than extremely luminous, beamed TDEs out to moderate redshift ($z \sim$ 1–2).

5 CONCLUSIONS

To summarize, during the acquisition of the final 3 Ms of the observations of the CDF-S 7-Ms survey, we detected an exceptional X-ray transient event, CDF-S XT1, at high significance. The X-ray light curve of CDF-S XT1 shows a fast rise [$\approx 100(1+z)^{-1}$ s] and a power-law decay time slope of $a = -1.53 \pm 0.27$, with little spectral variation and a peak flux of $F_{0.3-10\,{\rm keV,peak}} = 5.1 \times 10^{-12}$ erg cm^{-2} s^{-1}. The average spectrum can be modelled as an absorbed power law with a spectral slope of $\Gamma = 1.43^{+0.26}_{-0.15}$ and an absorption limit of $N_{\rm H} < 1.5 \times 10^{21}(1+z)^{2.5}$ cm^{-2}. The location of the event shows no prior or subsequent X-ray emission, allowing us to place 0.3–10 keV quiescent and precursor limits that are factors of 10^5 and 10^3 times fainter, respectively.

CDF-S XT1 is robustly matched, within ≈0.13 arcsec ± 0.26 arcsec, to a single optical counterpart, which lies in the CANDELS region and thus benefits from deep *HST*, *Spitzer* and ground-based imaging. The host is a resolved $m_{\rm R} = 27.5$ mag galaxy at $z_{\rm ph} = 2.23$ (0.39–3.21 at 2σ confidence). At this nominal redshift, the host SED is consistent with that of an $M_{\rm R} \sim -18.7$ mag, $\log M/{\rm M}_\odot \sim 8.0 \pm 0.2$, 1.15 ± 0.04 M$_\odot$ yr^{-1} dwarf galaxy. The inferred observed 2–10 keV peak luminosity of the event at this redshift is $(6.8^{+0.7}_{-1.6}) \times 10^{46}$ erg s^{-1}.

The combination of the X-ray light-curve properties, non-recurrence to deep quiescent X-ray limits, robust faint quiescent optical counterpart (or limits if somehow not associated) and lack of associated multiwavelength (optical/NIR, radio, >10 keV) transient emission to sensitive limits appears to exclude nearly all known

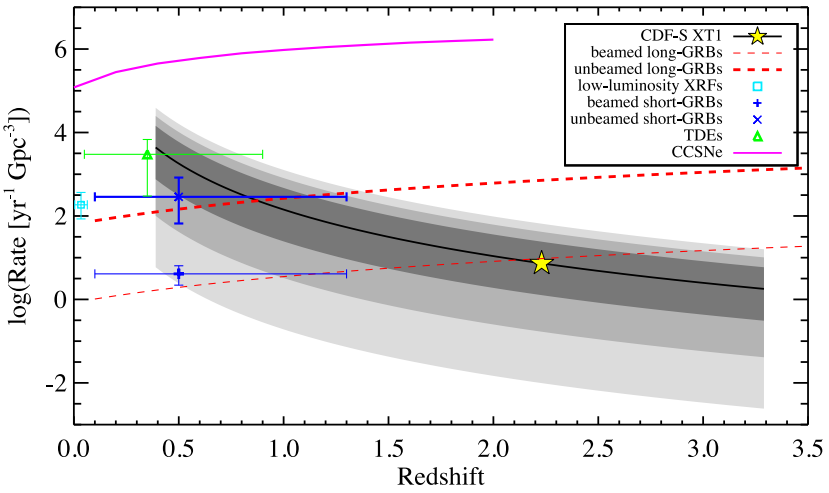

Figure 7. Volumetric rates as a function of redshift for several known transient classes compared to CDF-S XT1. For CDF-S XT1, the black curve denotes the rate based on the volume enclosed at a given redshift, adopting a range spanning the 95 per cent confidence limits of the photometric redshift of the associated host ($z_{\rm ph} = 0.39$–3.21). The light, medium and dark grey regions above and below the black curve denote the respective 3σ, 2σ and 1σ rate ranges at a given redshift. Also shown are a best-fitting broken power-law model (thin dashed red curve) representing the intrinsic beamed lGRB rate from Wanderman & Piran (2010) and Lien et al. (2014); the intrinsic unbeamed (orphan) lGRB rate (thick dashed red curve) assuming a beaming correction of 75 (Piran 2004; Guetta, Piran & Waxman 2005); the observed rate of low-luminosity XRFs (cyan square); the intrinsic beamed sGRB rate (blue plus sign) from Wanderman & Piran (2015); the intrinsic unbeamed (orphan) sGRB rate (blue X sign) assuming a beaming correction of 70 (Berger 2014); the intrinsic CCSNe rate (Lien & Fields 2009) and; the intrinsic TDE rate (Stone & Metzger 2016).

types of Galactic and extragalactic X-ray variables and transients. A few theoretical possibilities remain: an 'orphan' X-ray afterglow from an off-axis sGRB with weak optical emission; a low-luminosity GRB at high redshift with no prompt emission below ∼20 keV rest frame; or a strongly beamed TDE involving an IMBH and a WD with little variability. We stress that each scenario likely requires considerable fine-tuning to comply with all of the constraints. We encourage more efforts to explore and limit parameter space for CDF-S XT1. This situation bears parallels with the discovery of fast radio bursts (Lorimer et al. 2007), which represented a completely new source class, discovered by chance, with no clear-cut physical explanation. 'CDF-S XT1'-like events are indeed related to unbeamed/orphan sGRBs, then they will be relevant as sources of GW emission.

After failing to find any events identical to CDF-S XT1 in the *Chandra* Source Catalogue (comprised of the first 11 cycles of *Chandra*), we estimate a rate of 'CDF-S XT1'-like events as $< 4.2^{+9.7}_{-3.4}$ events deg^{-2} yr^{-1}. Although highly uncertain due to the small number statistics and wide photometric redshift range of its associated host, this potential rate appears crudely comparable at matched luminosity to that of unbeamed/orphan and low-luminosity lGRBs and sGRBs between $z \sim 0.4$ and 2.0, lending additional weight to a possible link with this transient class. Alternatively, the rate appears substantially higher than that expected for extremely luminous, beamed TDEs at moderate redshifts ($z \sim 1$–2), although this class of TDEs likewise suffers from small number statistics at present. Regardless of whether these events belong to an untapped regime for a known transient class, or represent a new type of variable phenomena, the predicted rates imply that 'CDF-S XT1'-like events should be a relatively common physical phenomenon that we are just beginning to observe or understand.

Although beyond the scope of this work, the peak 0.3–10 keV flux of CDF-S XT1 is sufficiently bright to be detected by several of the currently operating X-ray observatories. This could lead to the discovery of further similar transients and would certainly place more stringent limits on the rate estimates. For instance, incorporating the remainder of the *Chandra* archive would increase coverage by ∼50 per cent, while searching through the archives of *XMM–Newton* (FOV ≈ 0.25 deg^2, ≈260 Ms observed over 16 yr based on the master observation list catalogue) and *Swift* (FOV ≈ 0.15 deg^2, ≈250 Ms over 11 yr based on the master observation list catalogue) could increase the areal+temporal coverage by factors of ∼7.6 and ∼4.9, respectively. Moreover, these observatories could last another 5–15 yr, pending funding extensions. Alternatively, a few upcoming X-ray observatories may be able to make significant further progress. The *eROSITA* mission (Merloni et al. 2012) has an FOV of ≈0.833 deg^2 and sensitivity sufficient to detect transients like CDF-S XT1 in each one of its eight passes over the sky during the nominal four-year mission. Thus, *eROSITA* should effectively provide an equivalent coverage in sky area per time to the current *XMM–Newton* archive. Each individual 'pass' will provide an average exposure of ∼320 s, built up from a few short exposures every 4 h, such that rapid triggers can be performed. Given the relatively weaker hard energy response of *eROSITA* compared to *XMM–Newton*, however, rapid X-ray follow-up within 1–2 h will likely be necessary to properly characterize transients. Another prospect is the wide-field telescope planned for the Chinese Academy of Sciences' *Einstein Probe* (Yuan et al. 2015), which will have an FOV of $60^\circ \times 60^\circ$ and sensitivity of $\sim 10^{-11}$ in 1000 s. While this may be insufficient to detect CDF-S XT1 outright, it could potentially detect bright versions ($\gtrsim 10 \times$) if they exist. Taken together, we thus might expect at least a handful of 'CDF-S XT1'-like sources to be discovered in the next decade.

Looking further into the future, next-generation observatories like ESA's *Athena* (Barret et al. 2013), the proposed *X-ray Surveyor* (Gaskin et al. 2015) or any other wide-field X-ray observatory aim to provide FOVs of the order of ∼0.6–1 deg^2 and substantially better sensitivity than *Chandra* or *XMM–Newton*, so they may detect several dozen transients like CDF-S XT1 over their lifetimes. However, these observatories will be in a much better position to characterize the light curves in detail and probe factors of at least 10 deeper to study fainter (and perhaps more abundant) versions of

CDF-S XT1. In all of the above cases, 'CDF-S XT1'-like events will strongly benefit from rapid multiwavelength follow-up to help constrain their physical nature.

ACKNOWLEDGEMENTS

We acknowledge the staff of ESO, Gemini and *HST*, and in particular, Nancy Levenson, Blair Conn, Rodolfo Angeloni, Rene Rutten, Christian Hummel, Linda Schmidtobreick, Claus Leitherer, Denise Taylor and Shantavia Sturgis for their help in promptly accepting our DDT requests, preparing the observations and carrying them out. We thank Belinda Wilkes and the *Chandra* staff for help investigating *Chandra* instrumental effects. We would like to thank David Palmer, Hans Krimm, Ersin Göğüş, Yuki Kaneko, Alexander J. van der Horst, Shri Kulkarni and Avishay Gal-Yam for their help and stimulating conversations, and the *Fermi*-LAT team for providing LAT data products. We also thank the anonymous referee for several comments that help improve the manuscript.

We acknowledge support from CONICYT-Chile grants Basal-CATA PFB-06/2007 (FEB, ET, SS), FONDECYT Regular 1141218 (FEB) and 1160999 (ET), FONDECYT Postdoctorado 3140534 (SS), PCCI 130074 (FEB), 'EMBIGGEN' Anillo ACT1101 (FEB, ET); the Ministry of Economy, Development, and Tourism's Millennium Science Initiative through grant IC120009, awarded to The Millennium Institute of Astrophysics, MAS (FEB, FF, SS); Swiss National Science Foundation Grants PP00P2_138979 and PP00P2_166159 (KS); National Natural Science Foundation of China grant 11673010 (BL); Ministry of Science and Technology of China grant 2016YFA0400702 (BL); support from TLS Tautenburg, MPE Garching and DFG Kl/766 16-1 and 16-3 (DAK); Chandra X-ray Center grant GO4-15130A (BL, WNB); NASA through Hubble Cycle 22 grant HST-GO-14043 (FEB) awarded by the Space Telescope Science Institute, which is operated by the Association of Universities for Research in Astronomy, Inc., for NASA, under contract NAS 5-26555; World Premier International Research Center Initiative (WPI Initiative), MEXT, Japan (KM); Japan Society for the Promotion of Science (JSPS) KAKENHI Grant 26800100 (KM) and JSPS Open Partnership Bilateral Joint Research Projects (KM); 973 Programmes 2015CB857005 (JXW) and 2015CB857004 (YQX); CAS Strategic Priority Research Programme XDB09000000 (JXW, YQX); CAS Frontier Science Key Research Programme QYZDJ-SSW-SLH006 (JXW, YQX); NSFC-11421303 (JXW, YQX); National Thousand Young Talents programme (YQX); NSFC-11473026 (YQX); and Fundamental Research Funds for the Central Universities (YQX).

The scientific results reported in this paper are based in part or to a significant degree on observations made by the Chandra X-ray Observatory, on observations obtained at the Gemini Observatory acquired through the Gemini Observatory Archive and processed using the Gemini IRAF package, which is operated by the Association of Universities for Research in Astronomy, Inc., under a cooperative agreement with the NSF on behalf of the Gemini partnership: the National Science Foundation (United States), the National Research Council (Canada), CONICYT (Chile), Ministerio de Ciencia, Tecnología e Innovación Productiva (Argentina) and Ministério da Ciência, Tecnologia e Inovação (Brazil), is based on observations made with ESO Telescopes at the La Silla Paranal Observatory under programme ID 294.A-5005, and based on observations made with the NASA/ESA *HST*, obtained from the Data Archive at the Space Telescope Science Institute, which is operated by the Association of Universities for Research in Astronomy, Inc., under NASA contract NAS 5-26555. These observations are associated with programme HST-GO-14043. This work made use of data supplied by the UK Swift Science Data Centre at the University of Leicester. This work also made use of the Rainbow Cosmological Surveys Database, which is operated by the Universidad Complutense de Madrid (UCM), partnered with the University of California Observatories at Santa Cruz (UCO/Lick,UCSC). This research has made use of NASA's Astrophysics Data System Bibliographic Services.

REFERENCES

Abbott B. P. et al., 2016, Phys. Rev. Lett., 116, 061102
Atteia J.-L. et al., 1987, ApJS, 64, 305
Bade N., Komossa S., Dahlem M., 1996, A&A, 309, L35
Balberg S., Loeb A., 2011, MNRAS, 414, 1715
Barniol Duran R., Nakar E., Piran T., Sari R., 2015, MNRAS, 448, 417
Barret D. et al., 2013, in Cambresy L., Martins F., Nuss E., Palacios A., eds, Proc. Annu. meeting French Soc. Astron. Astrophys., SF2A-2013. p. 447
Barthelmy S. D. et al., 2005, ApJ, 635, L133
Becker A., 2015, Astrophysics Source Code Library, record ascl:1504.004
Berger E., 2006, ApJ, 648, 629
Berger E., 2014, ARA&A, 52, 43
Bianco F. B. et al., 2014, ApJS, 213, 19
Blandford R. D., Znajek R. L., 1977, MNRAS, 179, 433
Bloom J. S. et al., 2011, Science, 333, 203
Bochanski J. J., Hawley S. L., West A. A., 2011, AJ, 141, 98
Bower G. C., Metzger B. D., Cenko S. B., Silverman J. M., Bloom J. S., 2013, ApJ, 763, 84
Burlon D., Bannister K., Hancock P., Bell M., Murphy T., Huynh M., Gaensler B., 2014, Astron. Telegram, 6583, 1
Burrows D. N. et al., 2011, Nature, 476, 421
Campana S. et al., 2006, Nature, 442, 1008
Campana S. et al., 2011, Nature, 480, 69
Cash W., 1979, ApJ, 228, 939
Cenko S. B. et al., 2012, ApJ, 753, 77
Chandra P., Chevalier R. A., Chugai N., Fransson C., Irwin C. M., Soderberg A. M., Chakraborti S., Immler S., 2012, ApJ, 755, 110
Chevalier R. A., 1992, ApJ, 394, 599
Chevalier R. A., Irwin C. M., 2011, ApJ, 729, L6
Chincarini G. et al., 2007, ApJ, 671, 1903
Chincarini G. et al., 2010, MNRAS, 406, 2113
Ciolfi R., 2016, ApJ, 829, 72
Colgate S. A., Petschek A. G., 1981, ApJ, 248, 771
Comastri A. et al., 2011, A&A, 526, L9
Covino S. et al., 2013, MNRAS, 432, 1231
Dahlen T. et al., 2004, ApJ, 613, 189
Davis J. E. et al., 2012, in Takahashi T., Murray S. S., den Herder J.-W. A., eds, Proc. SPIE Conf. Ser. Vol. 8443, Space Telescopes and Instrumentation 2012: Ultraviolet to Gamma Ray. SPIE, Bellingham, p. 84431A
De Luca A., Tiengo A., D'Agostino D., Watson M., Haberl F., Wilms J., 2016, XMM-Newton: The Next Decade. p. 42, available at http://www.cosmos.esa.int/web/xmm-newton/2016-workshop
Dereli H., Boer M., Gendre B., Amati L., Dichiara S., 2015, preprint (arXiv:1506.05521)
Drout M. R. et al., 2011, ApJ, 741, 97
Eichler D., Livio M., Piran T., Schramm D. N., 1989, Nature, 340, 126
Ensman L., Burrows A., 1992, ApJ, 393, 742
Evans P. A. et al., 2009, MNRAS, 397, 1177
Evans I. N. et al., 2010a, ApJS, 189, 37
Evans P. A. et al., 2010b, A&A, 519, A102
Evans P. A. et al., 2014, ApJS, 210, 8
Falk S. W., Arnett W. D., 1977, A&AS, 33, 515
Frail D. A. et al., 2001, ApJ, 562, L55
Galama T. J. et al., 1998, Nature, 395, 670
Ganot N. et al., 2016, ApJ, 820, 57

Garnavich P. M., Tucker B. E., Rest A., Shaya E. J., Olling R. P., Kasen D., Villar A., 2016, ApJ, 820, 23
Gaskin J. A. et al., 2015, SPIE, 9601, 96010J
Gehrels N., 1986, ApJ, 303, 336
Gezari S. et al., 2006, ApJ, 653, L25
Gezari S. et al., 2015, ApJ, 804, 28
Ghirlanda G. et al., 2015, A&A, 578, A71
Giavalisco M. et al., 2004, ApJ, 600, L93
Glennie A., Jonker P. G., Fender R. P., Nagayama T., Pretorius M. L., 2015, MNRAS, 450, 3765
Grogin N. A. et al., 2011, ApJS, 197, 35
Guetta D., Piran T., Waxman E., 2005, ApJ, 619, 412
Guillochon J., Ramirez-Ruiz E., 2015, ApJ, 809, 166
Guo Y. et al., 2013, ApJS, 207, 24
Güver T., Özel F., 2009, MNRAS, 400, 2050
Hamuy M., 2003, ApJ, 582, 905
Harrison F. A. et al., 1999, ApJ, 523, L121
Horiuchi S., Beacom J. F., Kochanek C. S., Prieto J. L., Stanek K. Z., Thompson T. A., 2011, ApJ, 738, 154
Irwin J. A. et al., 2016, Nature, 538, 356
Jakobsson P. et al., 2012, ApJ, 752, 62
Jonker P. G. et al., 2013, ApJ, 779, 14
Kalberla P. M. W., Burton W. B., Hartmann D., Arnal E. M., Bajaja E., Morras R., Pöppel W. G. L., 2005, A&A, 440, 775
Kann D. A., Klose S., Zeh A., 2006, ApJ, 641, 993
Kann D. A. et al., 2010, ApJ, 720, 1513
Kann D. A. et al., 2011, ApJ, 734, 96
Klebesadel R. W., Strong I. B., Olson R. A., 1973, ApJ, 182, L85
Klein R. I., Chevalier R. A., 1978, ApJ, 223, L109
Koekemoer A. M. et al., 2011, ApJS, 197, 36
Kouveliotou C. et al., 1998, Nature, 393, 235
Laidler V. G. et al., 2007, PASP, 119, 1325
Lazzati D., Deich A., Morsony B. J., Workman J. C., 2016, MNRAS, preprint (arXiv:1610.01157)
Lee W. H., Ramirez-Ruiz E., 2007, New J. Phys., 9, 17
Levan A. J. et al., 2011, Science, 333, 199
Levinson A., Ofek E. O., Waxman E., Gal-Yam A., 2002, ApJ, 576, 923
Lien A., Fields B. D., 2009, J. Cosmol. Astropart. Phys., 1, 047
Lien A., Sakamoto T., Gehrels N., Palmer D. M., Barthelmy S. D., Graziani C., Cannizzo J. K., 2014, ApJ, 783, 24
Loeb A., Shvartzvald Y., Maoz D., 2014, MNRAS, 439, L46
Lorimer D. R., Bailes M., McLaughlin M. A., Narkevic D. J., Crawford F., 2007, Science, 318, 777
Luo B., Brandt N., Bauer F., 2014, Astron. Telegram, 6541, 1
Luo B. et al., 2017, ApJS, 228, 2
Margutti R., Bernardini G., Barniol Duran R., Guidorzi C., Shen R. F., Chincarini G., 2011, MNRAS, 410, 1064
Matzner C. D., McKee C. F., 1999, ApJ, 510, 379
Mazzali P. A. et al., 2006, ApJ, 645, 1323
Meegan C. A. et al., 1996, ApJS, 106, 65
Mereghetti S., Pons J. A., Melatos A., 2015, Space Sci. Rev., 191, 315
Merloni A. et al., 2012, preprint (arXiv:1209.3114)
Mészáros P., Rees M. J., 1997, ApJ, 476, 232
Metzger B. D., 2016, preprint (arXiv:1610.09381)
Metzger B. D., Piro A. L., 2014, MNRAS, 439, 3916
Metzger B. D., Giannios D., Thompson T. A., Bucciantini N., Quataert E., 2011, MNRAS, 413, 2031
Miller N. A. et al., 2013, ApJS, 205, 13
Mitra-Kraev U. et al., 2005, A&A, 431, 679
Modjaz M. et al., 2009, ApJ, 702, 226
Moriya T., Tominaga N., Blinnikov S. I., Baklanov P. V., Sorokina E. I., 2011, MNRAS, 415, 199
Narayan R., Paczynski B., Piran T., 1992, ApJ, 395, L83
Nicuesa Guelbenzu A. et al., 2012, A&A, 548, A101
Olausen S. A., Kaspi V. M., 2014, ApJS, 212, 6
Osten R. A. et al., 2016, ApJ, 832, 174
Palmer D. M. et al., 2005, Nature, 434, 1107
Pandey J. C., Singh K. P., 2008, MNRAS, 387, 1627
Park T., Kashyap V. L., Siemiginowska A., van Dyk D. A., Zezas A., Heinke C., Wargelin B. J., 2006, ApJ, 652, 610
Phinney E. S., 1989, in Morris M., ed., Proc. IAU Symp. 136, The Center of the Galaxy. Kluwer, Dordrecht, p. 543
Piran T., 2004, Rev. Mod. Phys., 76, 1143
Popov D. V., 1993, ApJ, 414, 712
Poznanski D., Gal-Yam A., Maoz D., Filippenko A. V., Leonard D. C., Matheson T., 2002, PASP, 114, 833
Pye J. P., Rosen S., Fyfe D., Schröder A. C., 2015, A&A, 581, A28
Racusin J. L. et al., 2009, ApJ, 698, 43
Rees M. J., 1988, Nature, 333, 523
Rhoads J. E., 1999, ApJ, 525, 737
Richardson D., Jenkins R. L., III, Wright J., Maddox L., 2014, AJ, 147, 118
Rosen S. R. et al., 2016, A&A, 590, A1
Rosswog S., Ramirez-Ruiz E., 2002, MNRAS, 336, L7
Sartore N., Ripamonti E., Treves A., Turolla R., 2010, A&A, 510, A23
Scargle J. D., Norris J. P., Jackson B., Chiang J., 2013, ApJ, 764, 167
Schawinski K. et al., 2008, Science, 321, 223
Schmitt J. H. M. M., Liefke C., 2004, A&A, 417, 651
Schulze S. et al., 2014, A&A, 566, A102
Skelton R. E. et al., 2014, ApJS, 214, 24
Soderberg A. M. et al., 2008, Nature, 454, 246
Starling R. L. C. et al., 2011, MNRAS, 411, 2792
Stone N. C., Metzger B. D., 2016, MNRAS, 455, 859
Sun H., Zhang B., Li Z., 2015, ApJ, 812, 33
Sun H., Zhang B., Gao H., 2017, ApJ, 835, 7
Svirski G., Nakar E., Sari R., 2012, ApJ, 759, 108
Tagliaferri G. et al., 2005, Nature, 436, 985
Taylor M. et al., 2014, ApJ, 792, 135
Tchekhovskoy A., Metzger B. D., Giannios D., Kelley L. Z., 2014, MNRAS, 437, 2744
Thornton D. et al., 2013, Science, 341, 53
Tinney C. G., Faherty J. K., Kirkpatrick J. D., Cushing M., Morley C. V., Wright E. L., 2014, ApJ, 796, 39
Tolstov A. G., Blinnikov S. I., Nadyozhin D. K., 2013, MNRAS, 429, 3181
Tominaga N., Morokuma T., Blinnikov S. I., Baklanov P., Sorokina E. I., Nomoto K., 2011, ApJS, 193, 20
Treister E., Bauer F., Schawinski K., 2014a, Astron. Telegram, 6603, 1
Treister E., Bauer F., Schawinski K., Conn B., 2014b, Astron. Telegram, 6650, 1
van Buren D., 1981, ApJ, 249, 297
van Eerten H. J., MacFadyen A. I., 2011, ApJ, 733, L37
van Eerten H., Zhang W., MacFadyen A., 2010, ApJ, 722, 235
van Putten M. H. P. M., Regimbau T., 2003, ApJ, 593, L15
van Velzen S. et al., 2016, Science, 351, 62
Villasenor J. S. et al., 2005, Nature, 437, 855
Wanderman D., Piran T., 2010, MNRAS, 406, 1944
Wanderman D., Piran T., 2015, MNRAS, 448, 3026
Wang X.-G. et al., 2015, ApJS, 219, 9
Watson D. et al., 2004, ApJ, 605, L101
Welsh B. Y. et al., 2007, ApJS, 173, 673
Wenger M. et al., 2000, A&AS, 143, 9
Williams P. K. G., Cook B. A., Berger E., 2014, ApJ, 785, 9
Woosley S. E., Heger A., 2012, ApJ, 752, 32
Xue Y. Q. et al., 2011, ApJS, 195, 10
Yamazaki R., Ioka K., Nakamura T., 2002, ApJ, 571, L31
Yuan W. et al., 2015, preprint (arXiv:1506.07735)
Zhang B., 2013, ApJ, 763, L22
Zhang B., 2014, ApJ, 780, L21
Zhang B., Mészáros P., 2004, Int. J. Mod. Phys. A, 19, 2385

[1] *Instituto de Astrofísica, Facultad de Física, Pontificia Universidad Católica de Chile, 306, Santiago 22, Chile*
[2] *Millennium Institute of Astrophysics (MAS), Nuncio Monseñor Sótero Sanz 100, Providencia, Santiago, Chile*

[3]*Space Science Institute, 4750 Walnut Street, Suite 205, Boulder, Colorado 80301*
[4]*EMBIGGEN Anillo, Av. Estaban Iturra, Box-160C, Concepción, Chile*
[5]*Departamento de Astronomía Universidad de Concepción, Casilla 160-C, Concepción, Chile*
[6]*Institute for Astronomy, Department of Physics, ETH Zurich, Wolfgang-Pauli-Strasse 27, CH-8093 Zurich, Switzerland*
[7]*School of Astronomy and Space Science, Nanjing University, Nanjing 210093, China*
[8]*Key laboratory of Modern Astronomy and Astrophysics (Nanjing University), Ministry of Education, Nanjing 210093, China*
[9]*Department of Physics, Durham University, Durham DH1 3LE, UK*
[10]*Department of Astronomy and Astrophysics, The Pennsylvania State University, 525 Davey Lab, University Park, PA 16802, USA*
[11]*Institute for Gravitation and the Cosmos, The Pennsylvania State University, University Park, PA 16802, USA*
[12]*Department of Physics, 104 Davey Laboratory, Pennsylvania State University, University Park, PA 16802, USA*
[13]*INAF – Osservatorio Astronomico di Bologna, via Ranzani 1, I-40127 Bologna, Italy*
[14]*Centro de Modelamiento Matemático, Universidad de Chile, Av. Blanco Encalada 2120 Piso 7, Santiago, Chile*
[15]*Thüringer Landessternwarte Tautenburg, Sternwarte 5, D-07778 Tautenburg, Germany*
[16]*Department of Astronomy, Kyoto University, Kitashirakawa-Oiwake-cho, Sakyo-ku, Kyoto 606-8502, Japan*
[17]*Kavli Institute for the Physics and Mathematics of the Universe (WPI), The University of Tokyo, Kashiwa, Chiba 277-8583, Japan*
[18]*Department of Physics, University Federico II, via Cintia 9, I-80126, Naples, Italy*
[19]*INFN – Sezione di Napoli, via Cinthia 9, I-80126 Naples, Italy*
[20]*Agenzia Spaziale Italiana Science Data Center, via del Politecnico snc, I-00133 Roma, Italy*
[21]*Lund Observatory, Department of Astronomy and Theoretical Physics, Lund University, Box 43, SE-22100 Lund, Sweden*
[22]*Department of Physics, University of North Texas, Denton, TX 76203, USA*
[23]*National Astronomical Observatory of Japan, Mitaka, Tokyo 181-8588, Japan*
[24]*Department of Physics, Faculty of Science and Engineering, Konan University, 8-9-1 Okamoto, Kobe, Hyogo 658-8501, Japan*
[25]*INAF Osservatorio Astrofisico di Arcetri, Largo E. Fermi 5, IFirenze, Italy*
[26]*Dipartimento di Fisica e Astronomia, Alma Mater Studiorum, Universitá degli Studi di Bologna, Viale Berti Pichat 6/2, I-40127 Bologna, Italy*
[27]*CAS Key Laboratory for Researches in Galaxies and Cosmology, Center for Astrophysics, Department of Astronomy, University of Science and Technology of China, Chinese Academy of Sciences, Hefei, Anhui 230026, China*

This paper has been typeset from a TEX/LATEX file prepared by the author.